CHAPTER

5

LABORATORY EXAFS FACILITIES

D. C. KONINGSBERGER

Laboratory for Inorganic Chemistry and Catalysis
Department of Chemical Technology
Eindhoven University of Technology
Eindhoven, The Netherlands

5.1. INTRODUCTION

Chapter 4 describes how EXAFS measurements can be carried out using a synchrotron as source for x-ray radiation. The photon density (photons s^{-1} eV^{-1} $mrad^{-1}$) as calculated for an EXAFS beamline of a storage ring is about 10^5–10^6 times higher than the brightness produced by the bremsstrahlung of a rotating anode x-ray source (1). The actual photon flux (photons s^{-1}) available at the experimental EXAFS stations of existing synchrotron beamlines is in most cases lower than the figures calculated for the tangent point of the corresponding beamlines. The concrete shielding of the storage ring and the splitting of the beam port after the front end in several beamlines make it impossible to bring the experimental stations closer than 5–10 m. Therefore, optical elements like mirrors (see Chapter 4) have to be used to collect most of the horizontal and vertical divergence of the beam. X-ray optics is not always present in EXAFS beamlines and mostly slits are used to optimize the resolution leading to a decrease of the available intensity. This means that, in practice, the differences in photon flux between synchrotron and laboratory EXAFS facilities are less drastic. Moreover, for EXAFS measurements carried out in the transmission mode (see Fig. 5.1*a*) the maximum useful photon flux is limited. It has been measured (2) that for fluxes of about 5×10^8 photons s^{-1} the experimental noise is not determined anymore by the photon statistics but by the noise produced by the electronics of the detection stage. Therefore, one should not be too pessimistic beforehand about the possibility of performing EXAFS experiments with a laboratory facility.

In principle, EXAFS wiggles can be measured by making use of a simple bent LiF monochromator crystal, a standard x-ray tube, and a commercially available Θ, 2Θ goniometer. However, with this setup measuring times for undiluted materials amount to days, with resolutions not better than 20 eV. The use of cryostats or sample cells is very difficult if not impossible. The obtained signal-to-noise ratio and the actual resolution of this type of EXAFS spectrometer make a reliable analysis of the structural parameters of the first-shell difficult, whereas higher coordination shells are hardly resolved in the Fourier transform of the experimental data.

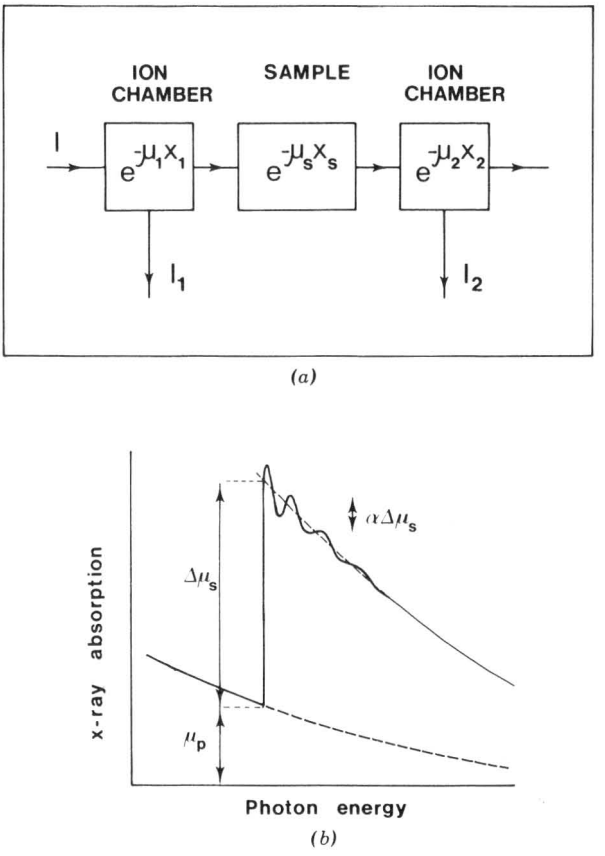

Figure 5.1. (*a*) Detection system for EXAFS in transmission mode. (*b*) An x-ray absorption spectrum ($\Delta\mu_s$ = absorption step due to sample; μ_p = pre-edge absorption, $\mu_s = \Delta\mu_s + \mu_p$).

The aim of this chapter is to demonstrate that good quality EXAFS data can be collected with in-house EXAFS facilities if these systems fulfill the demands that nowadays have to be made with regard to resolution, photon flux, feasibility, and foolproofness. It will be shown that with high quality curved monochromator crystals resolutions of 4–10 eV can be obtained, which give good quality EXAFS data. Intensities can be high enough to realize a signal-to-noise ratio better than 20–1 within scan times in the order of 1 to 20 h. The moving parts of the EXAFS spectrometer have to be especially designed so that the Rowland circle focusing geometry will maintain a positioning accuracy with a resettability in the order of 5 μm, and still allowing a 20–25-kg weight on the sample stage.

Motor positioning and position read out have to be computer controlled. To allow a broad spectrum of energies with emphasis on optimal resolution or on optimal intensities different types of good quality curved monochromator crystals must be available. A rapid change to a different type of monochromator crystal must be possible without new tedious alignment procedures.

Synchrotronlike intensities and resolutions have been claimed in the literature for laboratory EXAFS facilities (3). Some remarks have to be made concerning this optimism: (a) One has to realize that the photon flux of an EXAFS station on a synchrotron beamline is normally within a bandpass of 3 eV. A comparison of the Fourier transforms of synchrotron with laboratory EXAFS data will readily reveal the degrading influence of the resolution on the intensity of the peaks of the different coordination shells. (b) The statistics of EXAFS data obtained with the same resolution on the same sample should be compared for both the synchrotron and the laboratory setup with the same number of data points per spectrum and the same counting time per data point. (c) For a real comparison, the x-ray spot on the sample also has to be the same for both types of spectrometers. (d) Optimal resolution (~ 3 eV) is necessary on laboratory EXAFS systems, to detect the characteristic features present in the absorption edges. This automatically implies a low photon flux for a laboratory spectrometer. For EXAFS measurements the optimization of resolution and or intensity depends strongly on the type of information wanted or on the type of sample to be investigated. One should use a resolution of about 5–10 eV when information of higher coordination shells has to be obtained. High intensities with lower resolutions (10–20 eV) can be used when optimal signal to noise ratios are demanded on moderately diluted samples. Thus an optimized laboratory EXAFS spectrometer might have synchrotronlike resolutions although the intensities in most cases are still 10–100 times less, depending on the characteristics and the type of the synchrotron being used. The higher fluxes available at the storage rings make EXAFS experiments on highly diluted (< 25 mM) systems possible, which cannot be realized with a laboratory facility.

The demand for performing EXAFS measurements grew rapidly from 1975 to 1980 and is still growing. The synchrotron EXAFS facilities, which became available, stimulated the EXAFS community to develop techniques that made the laboratory EXAFS spectrometer no longer a curiosity but a scientific instrument. The laboratory EXAFS spectrometer is in principle capable of performing a large class of experiments. To discuss and review all the possibilities a workshop on laboratory EXAFS facilities and their relation to Synchrotron Radiation Sources was organized by Prof. Stern, Washington State University, Seattle in April 1980 (4). Since then, new techniques and technologies have been developed and new laboratory EXAFS facilities have been built and published in the literature.

The aim of this chapter is to give a review of the latest developments. The possibilities, as well as the limitations, of laboratory EXAFS spectrometers will be described. These spectrometers can be constructed using the techniques and technologies nowadays available in well-equipped workshops of universities and industries. A detailed discussion will be given (Section 5.2) about the specifications of laboratory EXAFS facilities. The different components of the laboratory EXAFS system, such as x-ray source, crystals, and detectors, are discussed in Section 5.3, with an emphasis on the quality of the mechanism that has to hold the Rowland circle configuration. Section 5.4 deals with the resolution as calculated for two different types of monochromator crystals (Johann, Johansson) including the important contribution caused by the finite dimension of the focal spot. A survey of a selected number of laboratory made EXAFS spectrometers as described in recent literature will be given in Section 5.5. Section 5.6 compares the laboratory with the synchrotron EXAFS facilities. A summary and conclusions are given in Section 5.7.

5.2. SPECIFICATIONS

5.2.1. Signal-to-Noise Ratio, Photonflux

To obtain structural information on a large class of different samples, laboratory EXAFS spectrometers have to produce a minimum useful photon flux. The relation between the photon flux and the signal-to-noise ratio for a transmission EXAFS experiment will be derived in the following.

The detection system for a transmission EXAFS experiment is given in Fig. 5.1(a). The ionization chambers have absorption coefficients μ_1 and μ_2, with chamber lengths x_1 and x_2, respectively. The sample has a thickness x_s and a linear absorption coefficient μ_s. I is the total number of photons collected per data point entering the first ionization chamber, while I_1 and I_2 represent the signals arising from the ionizations in the chambers. The absorption coefficient of the sample can be calculated from $I_2/I_1 = \exp[-(\mu_s x_s)']$. Due to the absorption coefficients of the ionization chambers, which enter in the measured signal I_1 and I_2, the determined absorption coefficient $(\mu_s x_s)'$ is not exactly equal to $\mu_s x_s$. The noise N in $(\mu_s x_s)'$ is given by

$$N = \sigma(\mu_s x_s)' = \left[(I_1)^{-1} + (I_2)^{-1}\right]^{1/2} \tag{1}$$

Assuming that the amplitude of the EXAFS signal is equal to a fraction α (the normal range for α is $0.01 < \alpha < 0.1$) of the edge jump $\Delta\mu_s x_s$ (see Fig. 5.1*b*)

the signal S can be represented by $S = \alpha\,\Delta\mu_s x_s$. The relation between the signal-to-noise ratio (S/N) and I can now be derived:

$$\frac{S}{N} = \frac{(I)^{1/2}\,\alpha\Delta\mu_s x_s}{\left\{\left(1 - \exp\left(-\mu_1 x_1\right)\right)^{-1} + \exp\left(\mu_s x_s + \mu_1 x_1\right)\left(1 - \exp\left(-\mu_2 x_2\right)\right)^{-1}\right\}^{1/2}} \tag{2}$$

An optimum S/N is obtained with $\mu_1 x_1 = 0.25$, $\mu_2 x_2 = \infty$, and $\mu_s x_s = 2.55$. Using these values, we obtain the total number of photons I necessary to get a certain signal-to-noise ratio (S/N) after t seconds collection time per data point:

$$I = 3.2\left(\frac{S}{N}\right)^2\left(\frac{\mu_s}{\alpha\,\Delta\mu_s}\right)^2 \tag{3}$$

Figure 5.2 gives the total number of photons (I) as a function of $\mu_s/\alpha\,\Delta\mu_s$ calculated for S/N values of 20/1 and 100/1. To derive reliable structural parameters from EXAFS data a minimum signal-to-noise ratio of about 20/1 is necessary (5). Maximum useful scan times per spectrum for laboratory EXAFS facilities are in the order of 20 h. Typical EXAFS spectra contain about

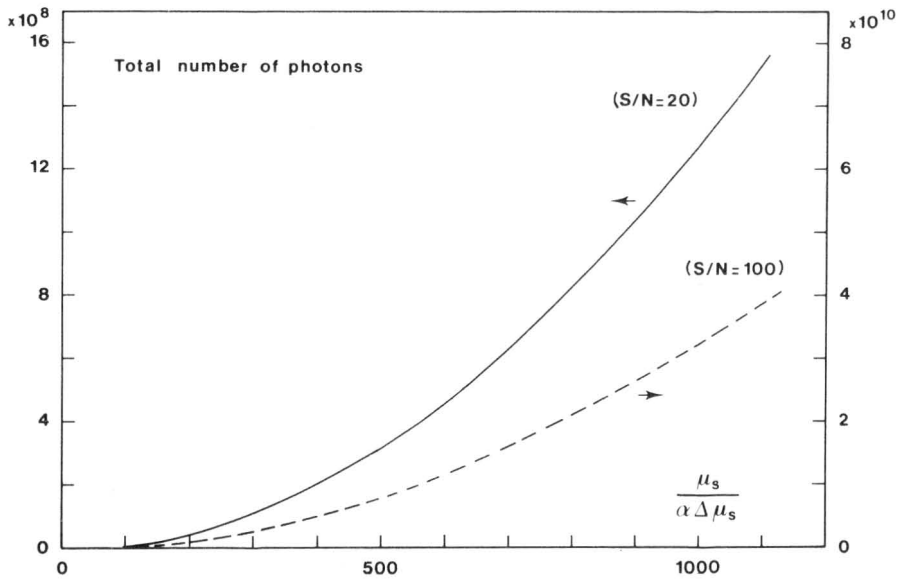

Figure 5.2. Total number of photons collected per data point $I = I_0 t$ as a function of $\mu_s/\alpha\Delta\mu_s$.

600 data points up to $k_{max} = 15$, leading to a maximum acceptable counting time per data point of 100 s. A large class of experiments can be carried out for $\mu_s/\alpha\ \Delta\mu_s \sim 500$. For a laboratory EXAFS spectrometer this implies a minimum useful photon flux I_0 of about 3×10^6 photons s^{-1}, accepting a maximum counting time of 100 s per data point. Typical values for bulk samples are $\alpha = 0.1$ and $\mu_s/\Delta\mu_s = 1$, which gives for $I_0 = 3.2 \times 10^6$ photons s^{-1} and 1 s collection time per data point a S/N value of 100/1 in a total counting time of 10 min.

5.2.2. Resolution Versus Intensity

5.2.2.1. Edge and Near-Edge Spectra

Optimum resolution is needed when all characteristic features of the absorption edge are of interest. This automatically implies the use of high index diffraction planes of the monochromator crystal (see Section 5.3.2), which have, however, lower reflectivities (6). Moreover, the smaller d values of these planes prescribe larger distances from the x-ray source (see Section 5.3.2), which in turn lead to lower photon density on the sample position. Figure 5.3 gives the x-ray absorption spectrum of the copper K-edge (8980.3 eV) of copper foil measured at room temperature at SSRL (Stanford University, USA) with a resolution of 2 eV. Measurements on a laboratory EXAFS spectrometer described in Section 5.5.2 equipped with a Johann-type curved ($R = 0.5$ m) Si(400) monochromator crystal resulted in a copper K-edge spectra, which are given in Fig. 5.3 as a function of the resolution of the spectrometer. The resolution can be degraded by increasing the spot size (in horizontal sense) on the Johann monochromator. The mentioned resolutions are calculated from linewidth measurements on the characteristic tungsten impurity lines present on the bremsstrahlung of the molybdenum anode. The results presented in Fig. 5.3 show that a resolution of 2 to 4 eV is necessary to measure edge and near-edge spectra. Resolutions of 2 eV at the copper-edge have been claimed in the literature for laboratory EXAFS spectrometers, using third-order reflections of Ge(111) (7) or Si(111) (8) and fourth order of Si(220) (9). With these higher-order reflections the available intensities are relatively low ($I_0 \sim 10^4$ photons s^{-1}). However, scan times for these types of edge spectra are still within 1–2 h (7–9), which is quite acceptable.

5.2.2.2. High Intensity and Reliable EXAFS Information

The photon density N_d (number of photons s^{-1} cm^{-2}) is inversely proportional to ℓ^2 where ℓ is the x-ray beam path length from focal spot to the sample. Using the formulas given in Section 5.3.2, the relation between the photon density N_d

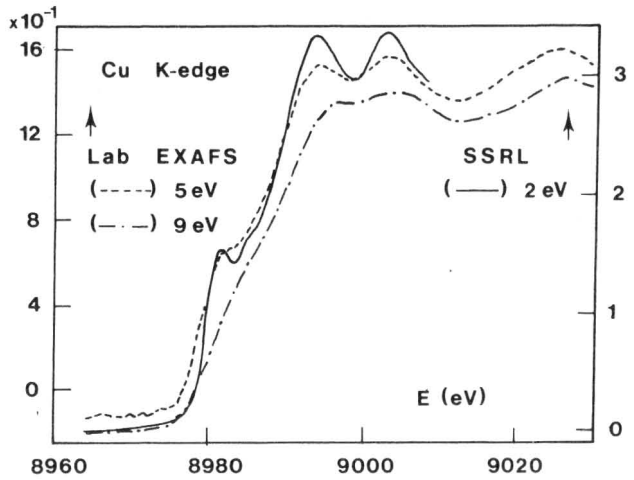

Figure 5.3. Copper *K*-edge spectra of copper foil (8.3 μm) as a function of the experimental resolution (rotating anode 17 kV, 180 mA).

and the d spacing of the monochromator crystal placed on the Rowland circle can be expressed as:

$$N_d \approx \frac{1}{\ell^2} \approx \frac{E^2 d^2}{R^2} \tag{4}$$

High intensities resulting in short collection times can thus be obtained with a monochromator crystal having a high d value mounted on a Rowland circle configuration with a short radius R. As will be shown in Section 5.4 such a choice (high d value, short radius) automatically leads to a low-energy resolution of the spectrometer. Therefore, a compromise must be made between intensity and resolution, which immediately puts forward the question, which kind of resolutions are acceptable for deriving reliable structural EXAFS information.

The influence of the experimental resolution on the peaks present in the radial structure function derived from the EXAFS data has been investigated in the following. Model EXAFS functions containing Pt–Pt (R_1 = 2.77 Å, R_2 = 5 Å) and Pt–O (R_1 = 2.05 Å, R_2 = 4 Å) coordinations have been calculated applying Eq. (4) of Chapter 6, Section 6.3.2. The phase and backscattering amplitude of the Pt–Pt and Pt–O absorber–scatterer combinations were obtained from EXAFS measurements on Pt-foil and $Na_2Pt(OH)_6$ (10).

These measurements were carried out at SSRL with a resolution of about 2–

3 eV. The influence of the experimental resolution on the actual EXAFS signal $\chi(E)$ can be simulated by

$$\chi'(E') = \int_{-\infty}^{+\infty} g(E', E)\chi(E)\, dE \tag{5}$$

with $\chi'(E')$ the simulated "measured" signal. A Gaussian type function was chosen to represent the experimental resolution function:

$$g(E', E) = \frac{1}{(2\pi\tau^2)^{1/2}} \exp\left(-\frac{(E - E')}{2\tau^2}\right) \tag{6}$$

The full width at half-maximum (FWHM) of this function is $2\sqrt{2 \ln 2}\,\tau$. Figure 5.4 gives the EXAFS functions and the corresponding Fourier transforms for the Pt–Pt and Pt–O coordinations as a function of $\Delta E = [(\Delta E)^2_{\text{SSRL}} + (\Delta E)^2_{\text{conv}}]^{1/2}$. The quantitative results as summarized in Table 5.1 make clear that an experimental resolution of 10 eV is a maximum value that can be allowed in order to derive reliable information of higher coordination shells. With a resolution of about 20 eV the peak of the first neighbor shell degrades to about 20%. If only information about the first coordination shell is desired the highest possible intensities can be used, since a relatively low resolution is sufficient to obtain structural information. For diluted systems a low-energy resolution has to be accepted in order to get a reasonable signal-to-noise ratio, which inevitably leads to a loss of structural information of higher coordination shells.

A decrease of the amplitude of a particular shell can be harmful when theoretical backscattering amplitudes and phases are used for the data analysis. However, amplitudes and phases can also be obtained from EXAFS data on model compounds with similar distances measured under the same conditions as the unknown material. Structural parameters obtained from these type of measurements on laboratory EXAFS spectrometers are reliable, although one still has to investigate possible errors.

5.2.3. Avoidance of Higher Harmonics

Higher harmonics in the x-ray beam form a very important class of thickness effects as discussed in Chapter 3. Higher harmonics have to be avoided as much as possible since they strongly distort the absorption edge and the EXAFS data leading to unreliable results.

When the x-ray absorption coefficient of a sample placed in a photon beam

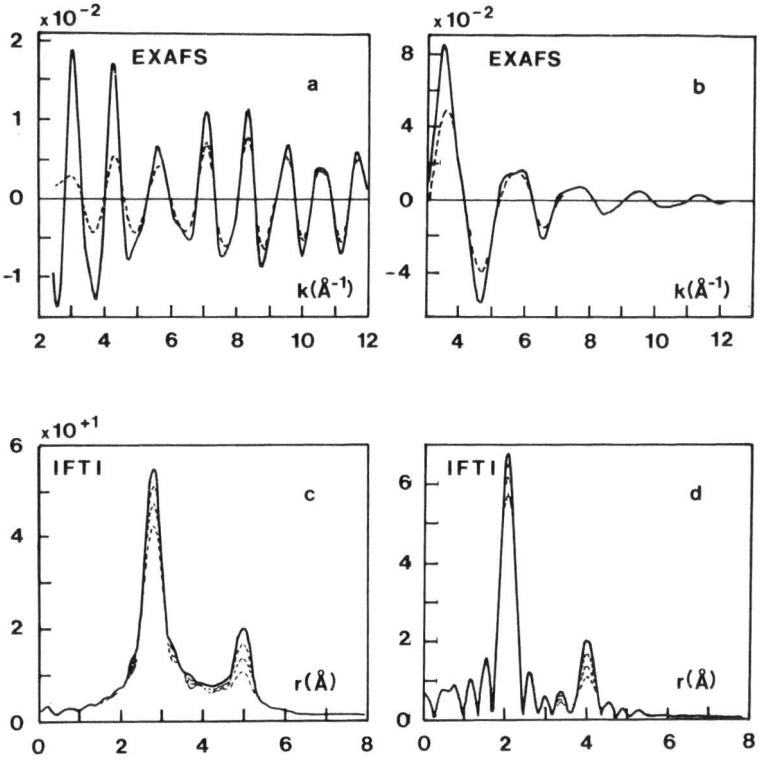

Figure 5.4. Influence of resolution on different coordination shells with different type of neighbors. (Pt—Pt: $N = 4$, $R = 2.77$ Å and $N = 4$, $R = 5$ Å; Pt—O: $N = 4$, $R = 2.05$ Å and $N = 4$, $R = 4$ Å) (*a*) Calculated Pt—Pt EXAFS (SSRL data: solid line; convolution with $\Delta E = 19.8$ eV: dotted line). (*b*) Calculated Pt—O EXAFS (SSRL data: solid line; convolution with $\Delta E = 19.8$ eV: dotted line). (*c*) Magnitude of Fourier transform (|FT|) of Pt—Pt EXAFS (SSRL data: solid line; convolution with $\Delta E = 9.5$, 14.7 and 19.8 eV: dotted lines). (*d*) Magnitude of Fourier transform (|FT|) of Pt—O EXAFS (SSRL data: solid line; convolution with $\Delta E = 9.5$, 14.7 and 19.8 eV: dotted lines).

Table 5.1. Influence of Resolution on EXAFS Data[a]

Total Resolution	Convolution		Pt-Pt		Pt-O	
			2.77(Å)	5(Å)	2.05(Å)	4(Å)
ΔE (eV)	ΔE_c (eV)	τ (eV)	D (%)	D (%)	D (%)	D (%)
3	0	0	—	—	—	—
10	9.5	4	7.5	18	4.2	17
15	14.7	6.3	15	32	8.5	29
20	19.8	8.4	23	48	15.5	44

[a]D is the relative decrease of the amplitude of the corresponding peak in the Fourier transform.

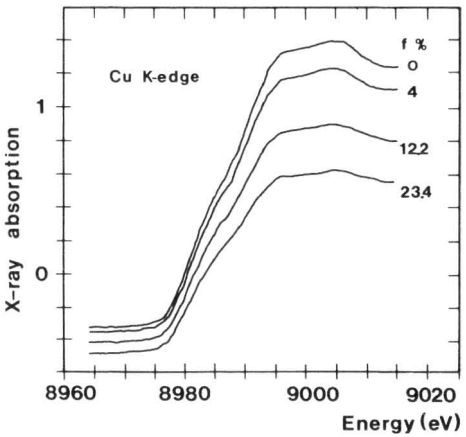

Figure 5.5. Influence of the presence of higher harmonics (fraction f) on the copper K-edge.

that contains higher harmonics is measured with ionization chambers (which are not energy discriminative), the energy response of the detection system is altered. Higher harmonics are hardly absorbed in the sample but contribute to the ionization currents in both chambers.

To investigate the effect of higher harmonics on the x-ray absorption spectrum a copper foil with a thickness of 8.3 μm was measured with a Si(400) monochromator crystal that allows the reflection of higher harmonic radiation. By varying the excitation voltage of the x-ray generator, the harmonic content can be changed. Figure 5.5 shows the influence of higher harmonics on the edge and near-edge spectrum of copper foil. The fraction of higher harmonics has been determined as described in ref. (11). Table 5.2 summarizes the results. Already a fraction of 10% higher harmonics has a large influence on the experimental results. The consequences of avoiding higher harmonics on the attainable photon flux, the choice of the type of monochromator crystal, and the performance of the rotating anode system will be discussed in Sections 5.3.1 and 5.3.3.

Table 5.2. Influence of the Fraction (f) of Higher Harmonics on the Copper Edge

kV	f(%)	$\Delta\mu x$	$\Delta\mu x/\Delta\mu x_{(f=0)} \times 100\%$
17	0	1.73	100
18	4	1.60	92
19	12.2	1.32	76
20	23.4	1.11	64

5.3. COMPONENTS

5.3.1. X-Ray Source

Although fixed sealed x-ray tubes can produce photon fluxes, which are useful for a certain class of EXAFS experiments, optimal photon fluxes for laboratory EXAFS spectrometers are obtained with rotating anodes. Fluxes generated by these type of x-ray sources are 10–15 times higher than the conventional fixed sealed tubes. The complexity of rotating anode generators sometimes limits reliable operation. When the mechanical performance of the anode assembly is not optimal, bearings and vacuum seals have to be renewed too often. The lifetime of the filaments will be short due to marginal vacuum conditions caused by the limited mechanical performance of the rotating anode. However, if rotating anode sources have an optimal performance (12) good vacuum conditions even at high tube powers can be maintained for very long running times in continuous operation (1–2 months using standard vacuum seals, 1–2 years with magnetic fluid type seals). Good vacuum conditions also lead to long lifetimes of the filaments. Choosing the rotating anode as x-ray source several specific points have to be considered, which will be discussed below.

5.3.1.1. High Currents at Low Voltages

The intensity of the bremsstrahlung spectrum intergrated over the whole energy range can be expressed (13) as

$$\text{Int} \approx ZV^2I \tag{7}$$

with Z the atomic number of the target and V and I the tube voltage and current, respectively. To generate high photon fluxes the rotating anode system must be able to provide high currents (200–300 mA), even when the excitation voltage has to be kept low (10–15 kV) to avoid the generation of higher harmonics. At low voltages the maximum current is severely reduced by the space charge in the electron beam. To operate the x-ray generator at high currents with low voltages the space-charge limit can be decreased by increasing the electric field between anode and cathode. This can be done by lowering the distance s (see Fig. 5.6) between cathode and anode. Figure 5.7 gives the V–I characteristic of a GX-21 (Elliot) rotating anode as obtained with a distance s of 6 mm.

5.3.1.2. Optimization of the Focal Spot

For an optimum resolution it is necessary to minimize the horizontal dimension of the focal spot on the rotating anode. The focusing of the electron beam is

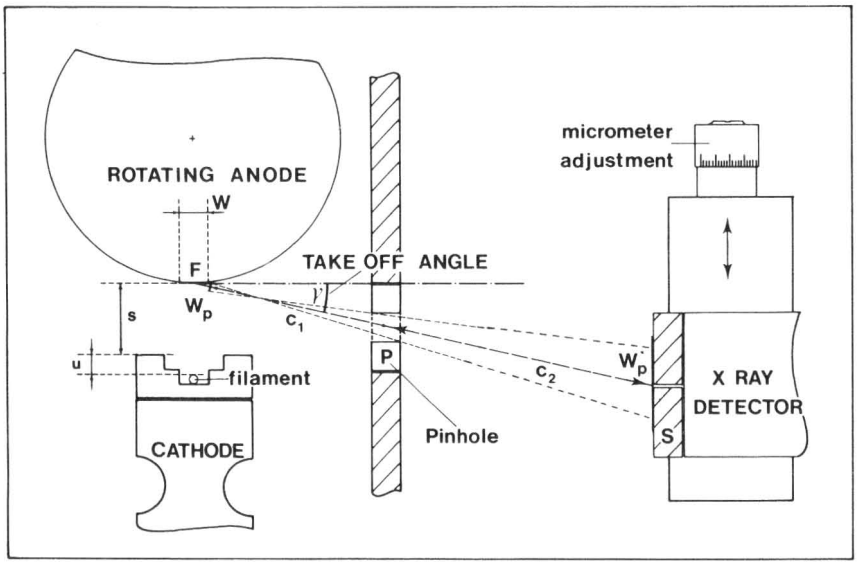

Figure 5.6. Configuration of the GX-21 (Elliot) rotating anode. (W = horizontal spot width, W_p = projected horizontal spot width, s = distance between cathode and focus cup, u = depth of filament in focus cup).

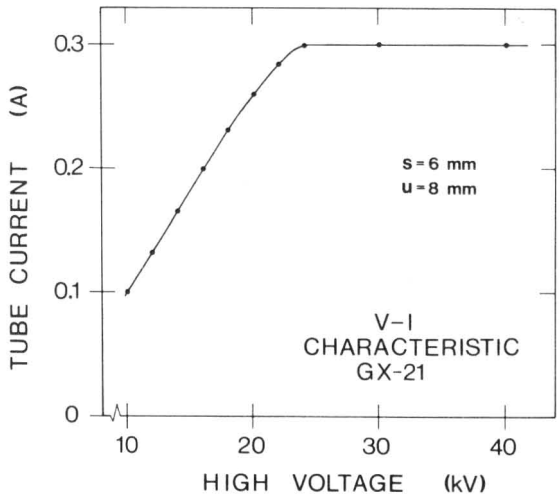

Figure 5.7. *V-I* characteristic of the GX-21 (Elliot) rotating anode. The maximum current limitation is caused by space charge between anode and cathode.

first of all dependent on the distance between cathode and anode, which determines the electric field and the amount of space charge. As discussed in the previous section this distance is prescribed by the voltage hold off requirement for avoiding higher harmonics. The filament is surrounded by a focusing cup, which has a specific shape in order to focus the electric field. The focal spot distribution can be optimized by changing the depth (u) (see Fig. 5.6) of the filament in the focus cup.

The focal spot distribution is very sensitive for small changes in u. It is also possible to focus the electron beam by applying a voltage between the filament and the focus cup (bias voltage). An increase in the bias level has a similar effect as bringing the filament deeper inside the focus cup. However, an increase in the bias level brings the space charge limit to higher tube voltages. Figure 5.8 shows focal spot distributions obtained for different values of s and u. The dimensions of the focal spot for high power operation are usually 0.5 mm (horizontal) $\times$ 10 mm (vertical).

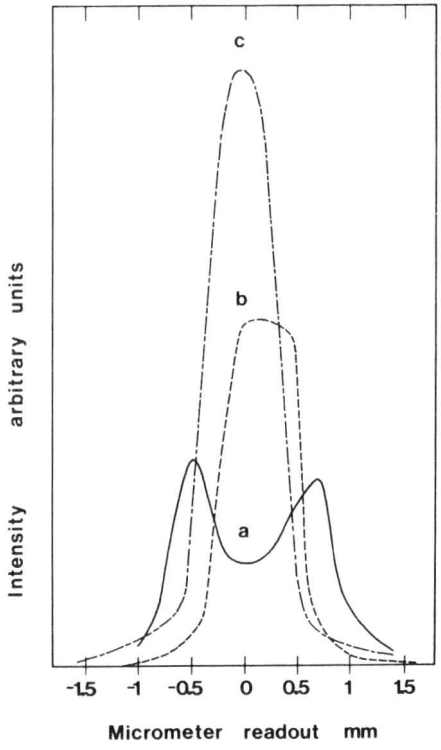

Figure 5.8. The intensity distribution of the x-ray focal spot as a function of the micrometer readout measured with the experimental setup as shown in Fig. 5.6. The following generator settings were used: (*a*) 20 kV, 200 mA, s = 9 mm, u = 7.5 mm; (*b*) 20 kV, 200 mA, s = 6 mm, u = 8 mm; and (*c*) 20 kV, 250 mA, s = 6 mm, u = 8 mm.

5.3.1.3. Choice of Target Material

The target material determines to a great extent the ranges of energies that are useful for EXAFS experiments. The energy regions of the high intense K_α lines and the other intense L_α lines cannot be used for taking good quality EXAFS data. Typical bremsstrahlung spectra for copper, molybdenum, and gold calculated (14) for an excitation voltage of 20 kV are given in Fig. 5.9. A good choice for the energy regions $4 < E < 10$ and $15 < E < 25$ keV is the high Z element gold, which cannot be used for $11 < E < 15$ keV where intense excitation L lines are present. The Mo anode is not useful at energies higher than the 17.5 keV (region of K_α lines and K-absorption edge). The molybdenum

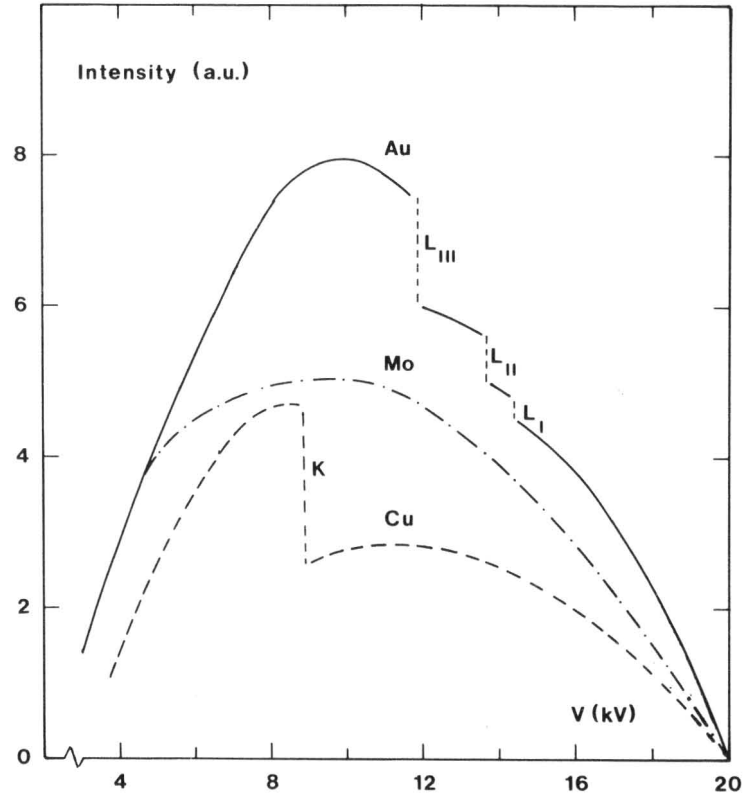

Figure 5.9. Bremsstrahlung spectra for copper molybdenum and gold calculated for an excitation voltage of 20 kV. The positions of the copper K edge and the gold L_{I}, L_{II}, and L_{III} absorption edges are indicated.

anode might replace the gold anode for $11 < E < 15$ keV. Another important advantage of using high Z elements as target material is the relatively high intensity produced by these elements at low take-off angles. A low take-off angle makes the effective horizontal focal spot size small, which in turn leads to better resolutions (see Section 5.4).

5.3.1.4. Flux Stabilization

Large variations of the incident flux are produced by intense excitation lines in the bremsstrahlung spectra of the x-ray tube. Even with an optimum choice of the target material spurious excitation lines will be present due to impurities in the target material. Also, slow evaporation of the tungsten filament gives a deposit on the hot anode and produces tungsten impurity lines in the incident x-ray spectrum. No problems occur when the response of the detector system is linear in a large dynamic range. Problems arise if pulse detectors are used in combination with large incident photon fluxes. Most pulse detectors start to become nonlinear at fluxes higher than 10^5 photons s^{-1}. Ionization chambers are linear in a large dynamic range. However, the current input range (saturation) of the current preamplifier is limited. It is, therefore, possible that the preamplifier may saturate when scanning through an excitation line. Some rotating anode x-ray generators are extremely suitable for adapting a feedback loop in the electronic circuit of the tube current stabilization system. The flux variations are monitored by the I_1 detector. The signal of the I_1 detector can be used as reference in the feedback loop circuit. Flux stabilization can give a dramatic improvement in the x-ray absorption spectrum obtained in a certain energy range (15) where contaminations with excitation lines are present (see Fig. 5.10).

5.3.2. Rowland Circle Configuration, Linear Spectrometer

The Rowland circle geometry is by far the best choice for monochromatization with curved crystals in order to achieve high photon fluxes. The Rowland circle configuration has been discussed in Chapter 4, Section 4.5.2.2. Normally, by changing the source and the sample simultaneously along the Rowland circle the crystal is tuned to different Bragg angles giving photons with different energies on the sample. This cannot be done due to the weight of heavy rotating anode x-ray sources and therefore special mechanical constructions for holding the Rowland circle configuration during the EXAFS scan have to be used.

Very useful is the linear spectrometer, which is presented schematically in Fig. 5.11. The situations for three different energies are drawn. The x-ray focal

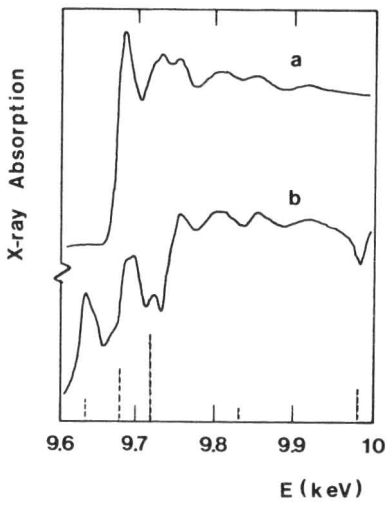

Figure 5.10. X-ray absorption spectrum of ZnO with (curve *a*) and without (curve *b*) x-ray flux stabilization. The positions of the major tungsten excitation lines are given.

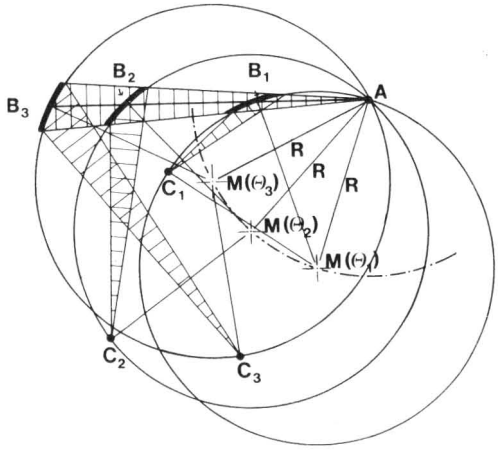

Figure 5.11. The linear spectrometer with positions for three different energies (for angles θ_1, θ_2, and θ_3). *A*: fixed focal point; *B*: center of monochromator crystal; *C*: sample position and *M*: center of Rowland circle.

spot (A) is the only fixed point on the Rowland circle. The center of the Rowland circle (M) itself moves along a circle with radius (R) with the focal spot as central point. The wavelength (λ) of the photons reflected by a monochromator crystal (with lattice spacing d) is linearly dependent on the distance (x) between focal spot and crystal:

$$\lambda = \frac{dx}{R} \tag{8}$$

This follows from the Bragg condition ($\lambda = 2d \sin \Theta_B$) with $x = 2R \sin \Theta_B$. The energy $E(kV)$ of the spectrometer is related to the lattice d spacing (Å) and the Bragg angle Θ_B by $E = 12.396/2d \sin \Theta_B$.

The accuracy (Δx) of the displacement (x) of the monochromator crystal along the x axis is then given by

$$\Delta x = \left(\frac{\Delta E}{E}\right) \frac{12.396\ R}{Ed} \tag{9}$$

To make steps of 1 eV at 15.000 eV a Si(111) ($d = 3.1353$) crystal has to be displaced along the x axis with increments of 10 μm for a Rowland circle with $R = 0.5$ m. The demands on the accuracies of the other parts of the linear spectrometer are related to this value. The moving parts of an EXAFS linear spectrometer should be free from any backlash. A good reproducibility of the energy scale for EXAFS measurements is necessary. By making use of electronic rulers a high positioning accuracy can be obtained. The read out of the position can be controlled by a computer, which makes the spectrometer fast and reliable with a good resettability.

The spectrometer should further fulfill the following demands:

1. An easy tunability that makes a realignment unnecessary if measurements have to be carried out in different energy ranges.
2. A rapid change of monochromator crystals without new tedious alignment procedures.
3. Easy and rapid change of the radius of the Rowland circle. This makes it possible to match the system to the curvature of the bent monochromator crystal. It also allows us to adapt the spectrometer to commercially available monochromator crystals.

4. A minimum load on the sample stage of about 25–30 kg weight without any relevant influence on the positioning accuracy.
5. Easy alignment with respect to:
   a. Take-off angle (see Fig. 5.6)
   b. Positioning of the focal point of the x-ray source onto the Rowland circle perpendicular to the used vertical focus.

5.3.3. Monochromator Crystals

The most critical part of the laboratory EXAFS facility is a curved monochromator crystal of high quality. For the Rowland circle geometry (radius R) two types of curved crystals are suitable (a) Johann: diffraction planes bent with radius $2R$, (b) Johansson: idem as (a) but also ground with radius R (see Chapter 4, Fig. 4.16). Optimal resolution with a high intensity can be obtained with Johansson type crystals. However, it is difficult to manufacture (bend, grind, and polish) an undistorted Johansson crystal, which makes the Johann type crystal worthwhile as an alternative. Single crystalline silicon and germanium material of large dimensions and of high quality are commercially available. Commercial sources for silicon and germanium Johansson type crystals are mentioned in recent literature (7, 8, 16). It has to be noted that the EXAFS monochromator crystals must be cut very carefully from the bulk material, in order to have no difference in angle (α) between the surface normal and the normal of the diffraction planes ($\alpha < 0.05°$) (15).

A value of 0.5 m for the radius of the Rowland circle takes care of a good compromise between the demands on resolution, high quality curved crystals and dimensions of the linear spectrometer. Using this R value, the type of index planes and the d value of these planes determine which type of monochromator crystal is most suitable to fulfill the requirements of harmonic rejection, resolution, intensity, or both. Ge(111) crystals are suitable for high intensities and medium resolutions for $4 < E < 7$ keV, whereas Ge(311) is extremely useful for $7 < E < 11$ keV. A Si(311) monochromator is the best choice for high intensities and medium resolution for $11 < E < 15$ keV.

Different methods for bending crystals have been described in the literature (17–22). Figure 5.12 shows the crystal bender as developed by Maas and Brinkgreve (12). A Si(400) crystal (thickness 400 μm) has been glued onto a U-shaped backing block of a well defined thickness and made of a special selected material. By pushing the ends of the U-shaped backing block in opposite directions, the monochromator crystal is bent along a very defined cylindrical surface (measured deviation from $2R = 1$ m is less than 5 μm). The copper-absorption edge spectra as given in Fig. 5.2 were measured with this type of crystal and bender.

5.3.4. Detectors

An extensive review of detectors suitable for laboratory EXAFS spectrometers has been given in ref. (23). Only the most relevant information of the gas proportional counter and the ionization chamber will be briefly discussed here.

Normal gas proportional counters can handle count rates up to 10^6 s^{-1} in the transmission mode. An important advantage of proportional counters is their energy discrimination. Higher harmonics can be rejected, which permits operation of the x-ray tube at higher voltages leading to higher photon fluxes. Multiwire proportional counters with separate electronics for each wire might be used to deal with count rates higher than 10^7 s^{-1}. Great care should be taken to the position and the maximum photon flux of each independent wire system.

Ionization chambers cannot discriminate against higher harmonics but their linearity makes them useful in a large range of photon fluxes (10^5–10^8 s^{-1}). Good, rigid, noise free ionization chambers can easily be built in a standard equipped workshop. Power supplies should have a voltage stability of 1 on 10^4, whereas current amplifiers should be used with extremely low-noise characteristics ($< 10^{-14}$ A). The best operation conditions are guaranteed when the current preamplifier is mounted directly on the ionization chamber with a very short connection wire between collection plate and preamplifier input. Low noise current preamplifiers can be commercially obtained. Special attention should be paid to the material used for the resistance (and capacitor), which determines the amplification factor of the preamplifier.

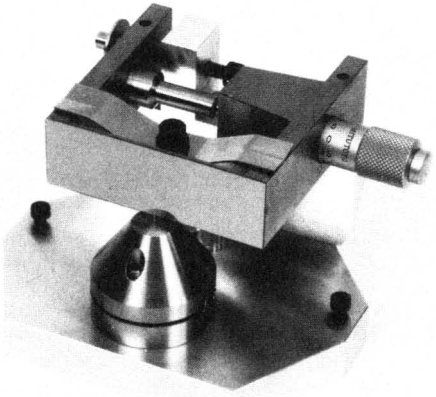

Figure 5.12. The Johann crystal bender developed by Maas and Brinkgreve (12).

5.3.5. Automating

Automating of EXAFS experiments is absolutely necessary for obtaining data that can be processed and analyzed at a later stage. A preliminary on line analysis should be possible (background subtraction and fast Fourier transformation) in order to investigate the quality of the EXAFS data for making a rapid decision for more and better scans. The reader is further referred to an excellent review of hardware and software considerations of EXAFS spectrometers given in the proceedings of the University of Washington workshop (4).

5.4. CRYSTAL OPTICS AND FOCUSING

5.4.1. Introduction

With an optimally mechanically constructed linear spectrometer, the curved monochromator crystal determines the attainable resolution and intensity. In this section the different contributions to energy resolution will be analyzed and the results of a Monte Carlo ray-tracing computer analysis (24) will be given. With a ray-tracing computer analysis it is possible to calculate the influence of different types of misalignments and to determine the tolerancies of the different components of the linear spectrometer. Both the Johann and the Johansson type of arrangements will be investigated. Based upon the calculations it is possible to select a particular crystal for a certain energy and to predict the intensity that belongs to a certain resolution.

The following contributions to the energy resolution of monochromator crystals can be distinguished:

1. Rocking curve ($\Delta\Theta_c$).
2. Dimensions of the crystal diffraction surface.
3. Finite dimensions of the source.

Berreman (25) computed the reflectance of symmetrically curved ideally perfect crystals in several wavelength ranges. He found that the rocking curves of Si(220) and Ge(220) are hardly affected by bending the crystals with a radius of 1 m. The rocking curves of Si(400) and Ge(400) are broadened by a factor 2 and 1.4, respectively. The influence of the crystal rocking curve ($\Delta\Theta_c$) will still be small in comparison to the contributions 2 and 3 [$\Delta\Theta_c \approx 0.4$ eV for Si(400) at 9000 eV]. The x-rays striking the monochromator crystal have a spread in incident angles $\Delta\Theta_g$ due to the geometry, which is determined by the dimensions of the crystal diffraction surface and the finite dimensions of the

x-ray spot. This spread in incident angles determines the resolution if $\Delta\Theta_g >> \Delta\Theta_c$. For maximum efficiency the rocking curve width $\Delta\Theta_c$ should be equal to $\Delta\Theta_g$. When geometrical effects dominate, the monochromator will reflect only a fraction of the photons incident in the bandwidth determined by $\Delta\Theta_c$. Diffraction efficiency can be increased by increasing the rocking curve of the crystal. By using, for instance, Ge(400) instead of Si(400), the intensity of the diffracted beam is higher due to the 2.5 times larger rocking curve width of Ge(400).

Some calculations of the energy resolution given in the literature (26) were based upon crystals with mosaic-type structures with large rocking curves (27). An analytical analysis of the Johann and Johansson focusing arrangements has been given by Lu and Stern (28) to show the practical usefulness of the Johann arrangement. For this analysis the finite dimensions of the source was not taken into account. The following calculations will include the finite dimension of the source assuming perfect crystals with $\Delta\Theta_c < \Delta\Theta_g$.

5.4.2. Analysis of Factors Determining the Energy Resolution

5.4.2.1. Horizontal Divergence

The main difference between the Johann and Johansson configuration is the contribution of the horizontal divergence. For a Johansson monochromator crystal all photons emitted by an x-ray point focus will have exactly the same incident angle with the crystal planes, which means that there are no energy aberrations in the horizontal plane. For the Johann configuration the horizontal aberrations are given by

$$\left(\frac{\Delta\Theta}{\Theta}\right)_{\text{hor}} = \frac{(-\cos\Theta)(1 - \cos\phi)}{(\sin\Theta)(\tan\Theta - \sin\phi)} \tag{10}$$

Θ is the angle between the crystal planes and the direction of the rays from the source to the origin of the crystal. ϕ is a parameter used to describe the position on the crystal surface ($\phi \approx w/2R$, with w the distance between a point on the crystal surface in the plane of the Rowland circle and the center of the crystal). By substituting the Bragg relation [E (keV) $= 12.396/2d \sin\Theta$] the relative energy resolution $(\Delta E/E)_{\text{hor}}$ can be given as a function of E, d, w, and R:

$$\left(\frac{\Delta E}{E}\right)_{\text{hor}} \simeq \frac{-w^2[(Ed)^2 - 38]}{307R^2} \tag{11}$$

By taking crystals with a smaller d spacing or a larger bending radius the

contribution of $(\Delta E/E)_{hor}$ can be diminished. For a normal experimental setup $(Ed)^2$ is larger than 38. Since $(\Delta E/E)_{hor}$ is a quadratic function of w the energy resolution function will therefore only contain aberrations to lower energy values. Equation (11) can be integrated along the crystal surface in order to obtain the mean and the standard deviation of the horizontal broadening factor for a certain value of w. More accurate results are obtained with the ray-tracing program. Figure 5.13 shows the energy resolution calculated with the ray-tracing program as a function of w at 10 and 15 keV for a Si(400) (d = 1.358 Å) Johann monochromator with R = 0.5 m. It can be seen that for small irradiated areas on the crystal the Johann crystal is comparable with the Johansson crystal. With a spectrometer with R = 0.5 m, the difference in horizontal energy broadening is only 2 eV at 10 keV when the Si(400) crystal is irradiated over 20 mm.

5.4.2.2. Vertical Divergence

Vertical divergence arises from x-rays that are reflected outside the (horizontal) plane of the Rowland circle. Normally, a (vertical) line focus in combination with a cylindrically bent crystal is used. The effect of vertical divergence, which is almost equal for the Johann and Johansson configuration is given by:

$$\left(\frac{\Delta\Theta}{\Theta}\right)_{vert} = \frac{(h-f)^2}{8R^2 \sin^2\Theta} \tag{12}$$

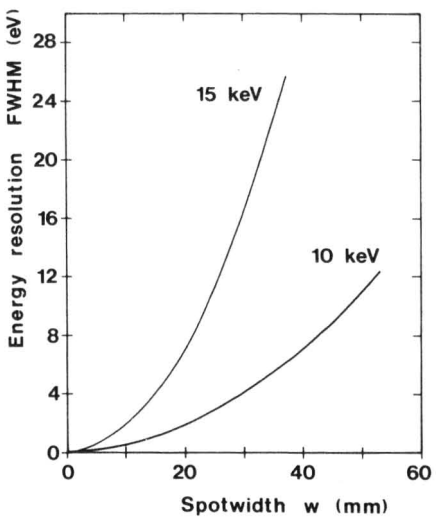

Figure 5.13. The influence of horizontal beam divergence. The energy resolution of a Johann monochromator has been given as a function of the distance (w) between the center of the crystal and a point on the crystal surface in the plane of the Rowland circle.

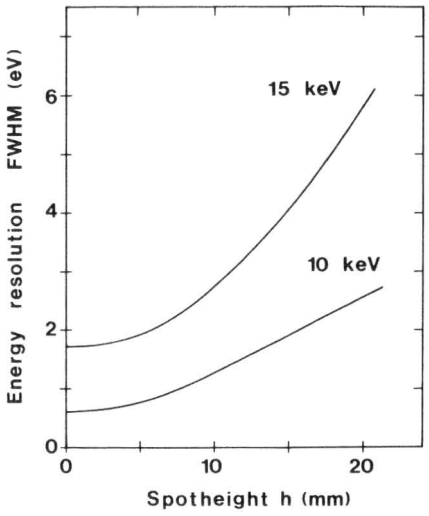

Figure 5.14. The influence of vertical beam divergence. The energy resolution of a Johann- or Johansson-type crystal monochromator has been calculated as a function of the vertical spot height (taken as the vertical distance along the crystal surface with respect to the plane of the Rowland circle).

with h the height of the crystal and f the height of the focal spot, both measured with respect to the origin of the crystal and focal spot, respectively. Using the Bragg relation, $(\Delta E/E)_{\text{vert}}$ can be calculated:

$$\left(\frac{\Delta E}{E}\right)_{\text{vert}} = \frac{(h-f)^2(Ed)^2}{307R^2} \tag{13}$$

$(\Delta E/E)_{\text{vert}}$ causes only aberrations to larger energies, since it is always positive. Figure 5.14 gives $(\Delta E/E)_{\text{vert}}$ as a function of the crystal spot height h. The ray-tracing program was used for the calculation. The total height of the x-ray source was taken 10 mm, with $R = 0.5$ m and $d = 1.353$ Å. It can be seen that for high energies and large vertical x-ray spot-sizes on the monochromator crystal the energy resolution is largely degraded.

5.4.2.3. Finite Focus Width

The width of the x-ray focal spot can have an important impact on the resolution function. This is especially the case at high energies when the crystal is positioned close to the x-ray source. Photons emitted from different positions on the finite source will be reflected under different angles by the same point on the crystal. Since the effects of the focus width are independent of the crystal configuration, a general expression can be derived:

$$\left(\frac{\Delta\Theta}{\Theta}\right)_{foc} = \frac{-\Delta \sin(\gamma + \frac{1}{2}\phi)\cos\Theta}{2R \sin(\Theta + \frac{1}{2}\phi)\sin\Theta} \tag{14}$$

with γ the take-off angle and Δ the half-width of the focal spot. The finite focus width causes a symmetric energy aberration. It can be seen from Eq. (14) that this aberration can be decreased by

1. Decreasing the width of the focal spot.
2. Decreasing the take-off angle.
3. Choosing the optimal side of the crystal, that is, the side of the crystal that has the largest distance to the focal spot.

Figure 5.15 gives the results of the ray-tracing program [$\Delta = 0.25$ mm, $R = 500$ mm, Si(400) as monochromator], showing that at high energies ($E > 15$ keV) a much better resolution can be obtained with a lower take-off angle.

5.4.2.4. Imperfect Grinding of the Crystal

As mentioned in Section 5.3.3, the normal vector of the diffraction planes does not necessarily have to coincide with the normal vector of the mechanical crystal surface. A mismatch between the normal vectors causes an additional deviation

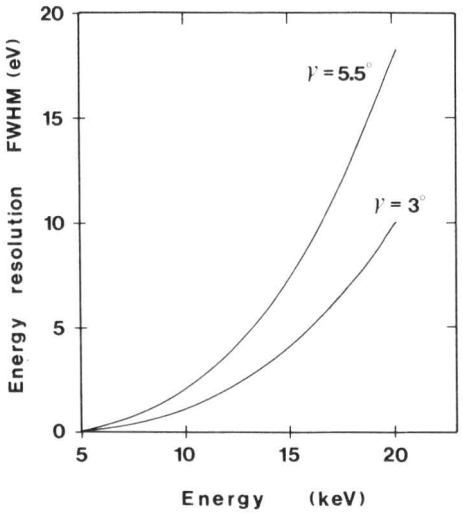

Figure 5.15. The influence of the finite focus width of the x-ray tube. The energy resolution has been determined as a function of the photon energy with the take-off angle as parameter ($\gamma = 5.5°$ and $3°$).

from the Rowland circle and thus a degradation in energy resolution. It can be shown that the deviation α between the normal vectors has to be lower than 0.2°. Larger deviations result in a tailing of the energy resolution function.

5.4.2.5. Angular Broadening

An effect that is of minor importance is the angular broadening (29). Due to the penetration of the photons in the monochromator crystal, photons are reflected from inner crystal planes. These planes are not exactly on the Rowland circle and have, therefore, different incident angles. The broadening is given by:

$$\left(\frac{\Delta\Theta}{\Theta}\right)_{\text{ang}} = \frac{-\cos\Theta}{\sin\Theta}\,(2\mu R\cos\Theta)^{1/2} \tag{15}$$

with μ the x-ray absorption coefficient of the crystal. The effect of angular broadening can normally (low value of μ) be neglected with respect to the effects mentioned previously.

5.4.3. Resolution as a Function of Energy

To get an impression of the total energy resolution of a particular Rowland circle configuration equipped with a specific type of crystal, Eqs. (10), (12), and (14) can be used to derive a general equation. This can be done by calculating the mean and the standard deviation of the various broadening factors. Assuming that all the energy resolution functions are Gaussian shaped, which is of course an approximation, the standard deviations have to be added in quadrature. It is possible to use the total standard deviation as a rough estimate for the total energy broadening. This may serve for a rapid comparison of various monochromator crystals.

The result of such a calculation is given in Fig. 5.16. The parameters used for the experimental setup are $R = 0.5$ m, take-off angle 5.5°, total focus height 10 mm, total focus width 0.5 mm, spot on crystal 10 mm (vertical) $\times$ w (mm) (horizontal) with w as variable. Acceptable resolution ($8 < E < 15$ keV) with an optimal curved crystal can be obtained with a Si(311) (Fig. 5.16*a*) Johansson-type monochromator crystal. The best resolutions are obtained with a Si(400) monochromator. The resolution of the Johann (Fig. 5.15*b*) and the Johansson (Fig. 5.16*c*) monochromators do not differ much when the crystal is irradiated with a spot of 20-mm width. However, when higher intensities are needed larger spot sizes are necessary and the Johann type is then not very useful anymore. Figure 5.16*d* gives the resolution of a Johann Si(400 crystal) irradiated with a

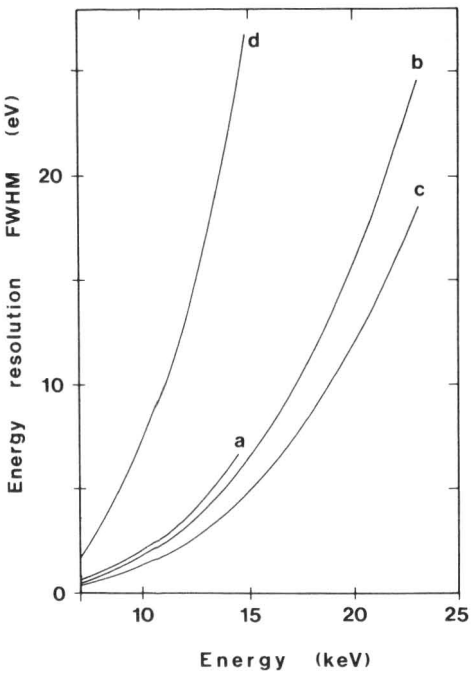

Figure 5.16. The total energy broadening as a function of photon energy for various monochromator crystals: (*a*) Johansson Si(311), w = 20 mm; (*b*) Johann Si(400), w = 20 mm; (*c*) Johansson Si(400), w = 20 mm and (*d*) Johann Si(400), w = 50 mm.

horizontal spot size of 50 mm. This curve may be compared with the results obtained for the Johansson crystal irradiated with horizontal spot size of 20 mm, since the resolution for a Johansson monochromator is independent of the horizontal spot size.

In the calculations mentioned previously it is assumed that all parts of the spectrometer are perfectly aligned. Due to a lack of vertical parallelism of source and crystal and also due to imperfectly ground or bent crystals an additional degrading of the resolution may be present. The experimental resolution can then be improved by using a receiving slit that is located on the Rowland circle where the reflected x-ray beam is converging. The width of this slit has to enter the calculation of the experimental energy resolution function. Such calculations were performed by Thulke et al. (8). They determined the actual resolution of their spectrometer equipped with a Ge(311) crystal, by measuring the FWHM of the copper $K_{\alpha 1}$ emission line. This line has a natural linewidth of about 2 eV. The actual energy resolution was found to be 4.5 eV, which was in excellent agreement with their calculations. Brinkgreve et al. (30) reported on measurements of the energy resolution of a laboratory EXAFS spectrometer with a

special (31) Si(111) Johansson crystal as monochromator. They used the characteristic x-ray emission lines of tungsten present in the bremsstrahlung spectrum of their x-ray generator. The presence of these lines is caused by the slow evaporation of the filament and the deposit on the anode. The width of three lines were measured ($WL_{\alpha 1}$: 8397.6 eV, $\Delta E_n = 6.5$ eV; $WL_{\beta 1}$: 9672.3 eV, $\Delta E_n = 6.9$ eV, and $WL_{\gamma 1}$: 11,285.9 eV, $\Delta E_n = 10.2$ eV) and from the broadening of these lines the actual energy resolution of the spectrometer was determined. The results are presented in Fig. 5.17. The geometrical configuration of the spectrometer is identical to the configuration used for calculation shown in Fig. 5.16. No entrance slits were used. The solid line in Fig. 5.17 represents the result of the calculation of the energy resolution function with the help of the ray-tracing program. There is a very good agreement between the theoretical and experimental results.

5.4.4. Intensity and Energy

The range of minimum and maximum energy of a linear spectrometer depend on the d-spacing of the monochromator crystal and the minimum and maximum anode-crystal distances of a particular setup.

The intensity that can be attained at a certain energy is dependent on several factors. As already mentioned in Section 5.2.2.2 high d values of the monochromator crystal and a short radius of the Rowland circle lead to a short distance between the anode-focal spot and the crystal. A short distance increases the photon density at the sample position. It also implies that by using a certain crystal the photon flux decreases going from the minimum to the maximum source-crystal distance. For the spectrometer described in (30) the photon flux changes then by a factor of 16. The intensity at a certain energy is further determined by the x-ray spot size on the crystal. The choice of these parameters (d-spacing, R-value, and spot size) is determined by a compromise between intensity and resolution.

The structure factor of the diffraction planes of a particular type of monochromator crystal is also important for the intensity that can be obtained at a certain energy. The reflectivity and thus the rocking curve depend on the structure factor of the index plane that has been used. As mentioned already in Section 5.4.1 the intensity of the diffracted beam can be increased by making use of germanium instead of silicon crystals due to the larger rocking curves of germanium. The structure factor also prescribes the maximum excitation voltage of the x-ray tube. This voltage has to be kept below the value, which starts to generate higher harmonics. For measuring copper EXAFS (~ 9 keV) 18 kV is a maximum value for a Si(400) crystal, whereas 27 kV can be used for Si(111) or Si(311). The structure factor for the (222) or (622) reflection is zero, implying

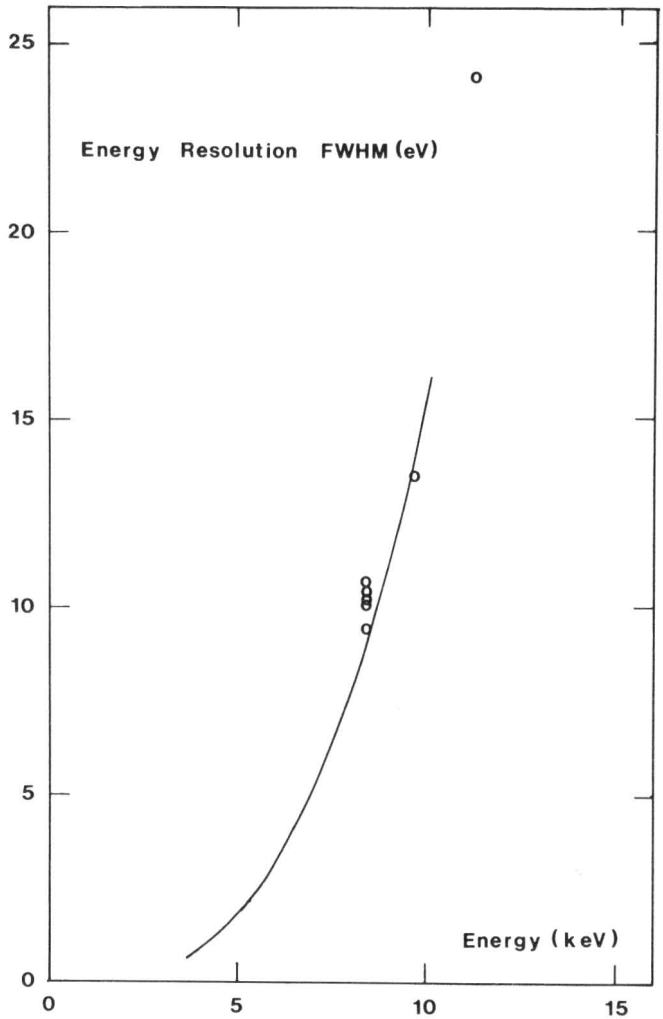

Figure 5.17. The energy resolution of the laboratory spectrometer (30) measured (open circles) as a function of photon energy using a special Si(111) Johansson monochromator. The solid line represents the calculated energy resolution.

no reflection of the first harmonic. This means that for Si(400) the optimal diffracted intensity at the copper *K*-edge is about 2.25 times lower than for Si(111) or Si(311).

5.5. LABORATORY EXAFS SPECTROMETERS

5.5.1. Mechanisms for Holding the Rowland Circle Configuration

Different mechanisms especially designed for holding the Rowland circle configuration for EXAFS spectrometers have been reported in the literature. In this section three systems will be described in more detail. These systems might fulfill the demands listed in Section 5.3.2.

Thulke et al. (8) use a combination of a single-axis goniometer (GO) and three translation stages (SC1, SC2, and SC3) to achieve optimal focusing and monochromatization using the principles of the linear spectrometer (see Fig. 5.18). For a curved crystal monochromator with bending radius $2R$ the distance x_c between source and crystal has to be changed according to:

$$x_c = 2R \sin \Theta_B \tag{16}$$

when the Bragg angle Θ_B is changed by rotating the crystal. Normally a receiving slit is used in front of the first ionization chamber. This slit is located on the Rowland circle on the point of convergence of the x-rays reflected from the crystal monochromator. The receiving slit has to be aligned at the same distance x_c from the crystal at an angle $2\Theta_B$ with the direction of the primary x-ray beam. The position (x_s, y_s) of the receiving slit is given by

$$x_s = x_c + x_c \cos 2\Theta_B \tag{17}$$

$$y_s = x_c \sin 2\Theta_B \tag{18}$$

The Rowland circle focusing geometry can be maintained during an EXAFS scan by changing x_c, Θ_B, and x_s, y_s according to Eqs. (16)–(18). This requires two motions of the monochromator crystal (x_c, Θ_B) and two of the receiving slit (x_s, y_s). The crystal (CR) is rotated (Θ_B) by the goniometer (GO) placed on the lowest translation stage (SC1), which moves according to Eq. (16). This translation stage moves at the same time the other two stages SC2 and SC3 with the detector platform according to the first term of the sum in Eq. (17). The second term of this sum $(x_c \cos 2\Theta_B)$ is realized by a movement of the upper

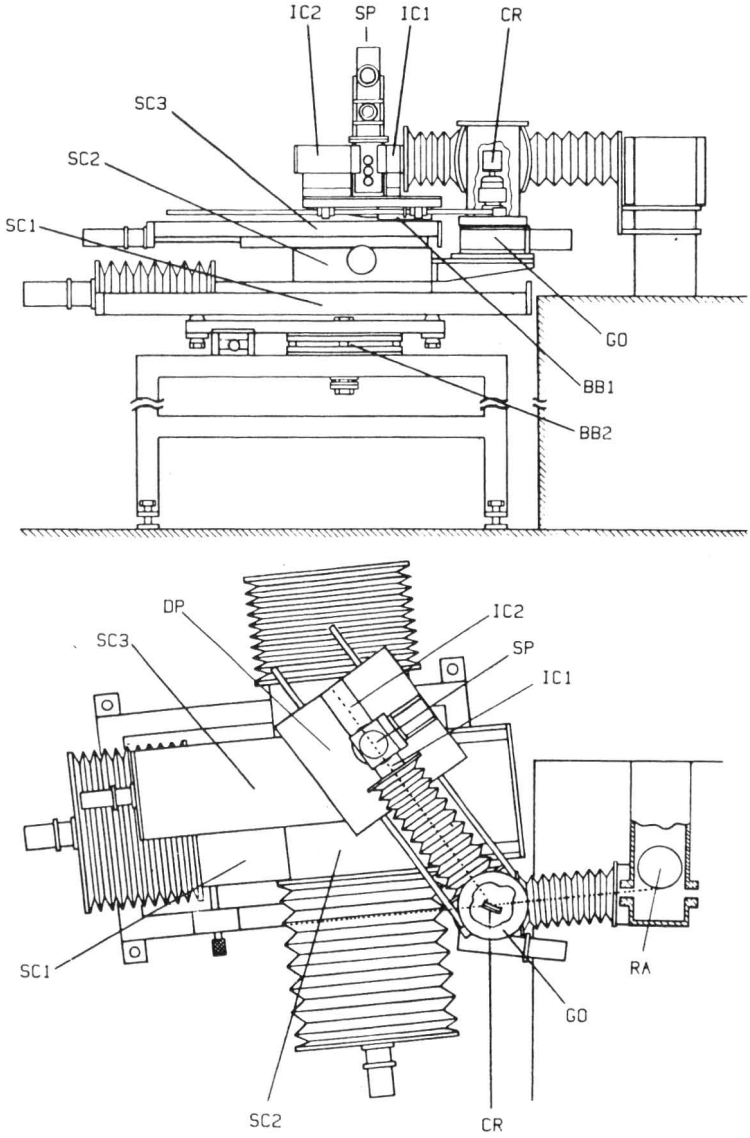

Figure 5.18. Side view (upper half) and top view (lower half) of the EXAFS spectrometer built by Thulke et al. (8). RA: rotating anode; CR: monochromator crystal; IC1 and IC2: ionization chambers; SP: sample cell; GO: single axis goniometer; SC1, SC2, and SC3: lower, intermediate, and upper sliding carriage, respectively; BB1 and BB2: axial ball bearings; DP: detector platform.

stage (SC3). The intermediate translation stage (SC2) takes care of the movement y_s perpendicular to x_s according to Eq. (18). The goniometer is driven by a stepping motor with minimum angle increments of 10^{-3} degrees. The translation stages are mounted on linear needle bearings of high accuracy, which are operated by 2.5-threads/cm backlash-free ball screws. The stages are driven by stepping motors set at 1000 steps/revolution. The net linear precision is better than 0.01 mm per 300 mm travel length, with a transverse tolerance of the movement of the carriage less than 0.004 mm per 100 mm displacement. The actual travel lengths are monitored by electronic linear scalars, with an accuracy of 0.003 mm over the full displacement. The net load capacity of the detector platform is 1 kN in extreme positions. With this design a physical fixed point below the focal spot on the anode is not required, which makes this setup especially suitable to be used in combination with a Rigaku rotating anode.

The spectrometer published by Tohji et al. (9) is based upon two translation stages driven by stepping motors and a sample–detector platform that can move freely in the horizontal plane floating above the base of the spectrometer by an air bearing. Figure 5.19 gives a schematic diagram of this construction. The focal spot of the x-ray generator, the center of the monochromator crystal and the receiving slit are positioned on the Rowland circle by two bars and three leads. The leads, L_1 and L_2, are set perpendicular to each other, such that the anode focal spot is located above the virtual intersection of the two leads. The

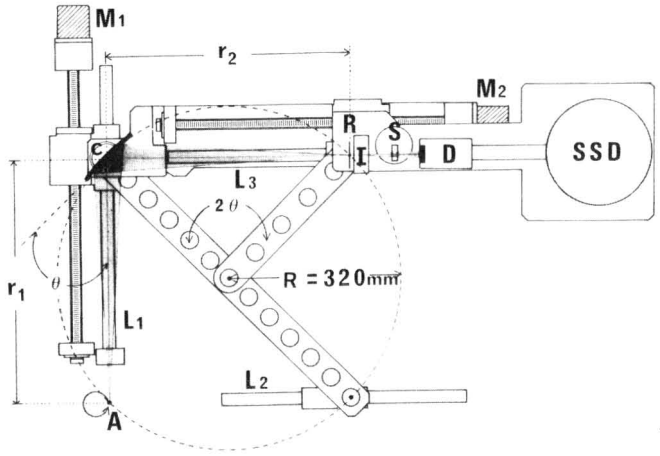

Figure 5.19. The EXAFS spectrometer published by Tohji et al. (9). A: rotating anode; C: monochromator crystal; R: receiving slit; I: ionization chamber; S = sample positioner; D: detector; M_1 and M_2: stepping motors; L_1, L_2, and L_3: leads.

monochromator is positioned at one end of the bar with fixed length $2R$, such that the normal on the crystal surface is parallel to the bar and goes always through the center of the Rowland circle. Both ends of this bar slide along the two leads. The end of this bar, where the crystal is located, is displaced by means of stepping motor M_1. This displacement causes the variation of the Bragg angle Θ_B. The other bar with fixed length R rotates at one end around the center of the Rowland circle, while the other end is connected to the sample–detector platform. This end is able to rotate around the axis determined by the position of the receiving slit. The sample–detector platform with receiving slit slides along lead L_3, which is driven by stepping motor M_2. This platform can move freely above the base of the spectrometer by means of the air bearing. When stepping motors M_1 and M_2 are scanning through an x-ray absorption spectrum the receiving slit follows on the Rowland circle the point of convergence of the x-rays reflected by the monochromator crystal. A smooth translation motion without clearance has been obtained by making use of a circulating ball linear bearing.

The linear spectrometer as described by Brinkgreve et al. (30) is shown in Fig. 5.20. The spectrometer is based upon a mechanism consisting of the following elements:

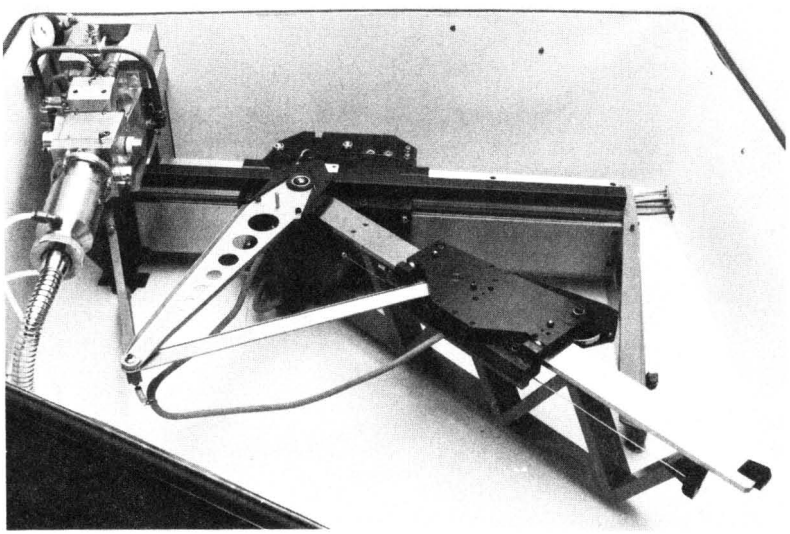

Figure 5.20. Photographic view on the EXAFS linear spectrometer designed and constructed by Brinkgreve et al. (30).

1. The main slide that moves along the main guide in order to change the distance between the x-ray focal spot and the monochromator crystal.
2. The monochromator support, which is attached to the main slide by means of a rotating axis.
3. The sample detector slide, which moves along a guide connected to the main slide by means of the same rotating axis as used for the monochromator support.
4. Three arms of equal length with one common central axis (center of the Rowland circle):
   —One arm from the anode source point.
   —The monochromator arm rigidly attached to the monochromator support.
   —The sample detector arm from the sample focal spot.

The elements described maintain the Rowland circle configuration as long as the distances from the x-ray source to the monochromator axis and from this axis to the sample focal spot are kept equal within the design specifications. The angle between the monochromator crystal and the x-ray beam changes during the displacement of the main slide along the main guide according to Eq. (16). The high positioning accuracy of the total mechanism has been achieved by paying full attention to the kinematical and statistical design specifications of the total layout and its components. In addition, all bearings and bearing points are preloaded in order to eliminate all virtual and actual clearance. Each slide is driven by transmission friction wheels that are coupled to a DC motor. By using DC motors and ruler systems of high mechanical resolution the positioning accuracy is realized by a computer electronic feedback system. With a radius $R = 0.5$ m of the Rowland circle and a Si(400) crystal ($d = 1.3567$ Å) "mechanical" incremental steps of 0.2 eV can be obtained with a resetability of ± 0.1 eV at the copper-edge (9 keV). The sample detector slide can easily accommodate a load capacity of 2.5 kN, without a relevant change in positioning accuracy.

5.5.2. A Survey of Spectrometers Known from the Literature

A survey of laboratory EXAFS spectrometers as known from the recent literature is given in Table 5.3. All systems are based upon a Rowland circle configuration with curved crystals (Johann or Johansson type) to be used as an energy scanning spectrometer. Question marks in Table 5.3. indicate that no information about a particular subject can be found in the corresponding paper.

Table 5.3. A Comparison of Laboratory EXAFS Facilities

	Cohen et al. (33)	Georgopoulos and Knapp (32)	Stern et al. (4), (24)	Khalid et al. (16)	Thulke et al. (8)	Williams (7)	Tohji et al. (9)
X-Ray source							
Standard (S)/Rot. anod (RA)	RA	RA	S	RA	RA	S	RA
Type	Rig. RU 200	Elliot GX-21	Picker	Rig. RU 200	Rig. RU 200	Rigaku	Rig. RU 200
Maximum power (kW)	12	15	1.2	12	12	2	12
Target material	Mo	Au	W, Ag	Mo	Au, Ag	Mo	Mo
Focal spot ($f \times W$ mm^2)	10 × 0.5	10 × 0.5	10 × 0.75	10 × 0.5	10 × 0.5	?	10 × 0.5
Take-off angle (°), Wp (μ)	6, 50	6, 50	4, 52	3, 30	6, 60	?, 40	6, 50
Rowland circle							
Radius (mm)	350	200	510	500	350	400	320
Fixed (F)/Adaptable (A)	F	F	?	A	A	A	?
Linear Spectrometer (LS)/ moving anode (MA)	LS	LS	MA	LS	LS	MA	LS
Number of motors	1	1	1	4	4	1	2
Position readout (Y/N)	N	N	N	N	Y	N	N
Load on detector stage (KN)	?	?	1.5	?	1	?	?
Monochromator crystals							
Johann (J), Johansson (JS)	JS	J	J	Flat/JS	JS	JS	JS
Material	LiF (220)	Si (400)	Si (400)	Si (311)	Si (111), Si (311) Ge (311)	Ge (111)	Si (220), LiF (220)
Commercial (Y/N)	?	?	Y	Y	Y	Y	Y
Dimensions ($h_c \times w_c$ mm^2)	25 × 25	?	?	30 × 50	10 × 40	20 × 127	20 × 50

Table 5.3. (*Continued*)

	Cohen et al. (33)	Georgopoulos and Knapp (32)	Stern et al. (4), (24)	Khalid et al. (16)	Thulke et al. (8)	Williams (7)	Tohji et al. (9)
Receiving slit							
Dimensions ($h_r \times w_r$ mm^2)	?	10 × 0.05	?	? × 0.01	10 × 0.15	12 × 0.076	? × 0.1
Focus on slit (Y/N)	Y	Y	Y	?	Y	Y	Y
Resolution							
A. EXAFS							
ΔE at E (eV)	9.5/8600	6/8980	5/8980	6.2/8397	4.6/8200	10.8/8200	?
Crystal	LiF(220)/JS	Si(400)/J	Si(400)/J	Si(311)/JS	Ge(311)/*JS*	Ge(111)/*JS*	LiF/JS
Measured	Zn $K_{\alpha 1}$ $K_{\alpha 2}$	?	?	W$L_{\alpha 1}$	Cu $K_{\alpha 1}$	Cu $K_{\alpha 1}$	?
Calculated	8.4	?	?	4.7	4.5	5.5	?
B. XANES							
ΔE at E (eV)	—	—	—	2.1/8980	2/8980	1.5/8200	2/8980
Crystal	—	—	—	Si(311)/2xFlat	Si(333)/JS	Ge(333)/JS	Si(440)/JS
Measured (M)/Estimated (E)	—	—	—	E	E	M	E
Figure copper-edge (Y/N)	—	—	—	Y	Y	Y (Cu $K_{\alpha 1}$)	Y

Intensity								
A. EXAFS								
Photon s^{-1}/energy (eV)		5×10^7/ 8980	4×10^7/ 7–10(keV)	5×10^5/ 8980	— —	5×10^6/ 8200	6×10^6/ 8980	3×10^5/8980
Crystal		LiF(200)	Si(400)	Si(400)	—	Ge(311)	Ge(111)	LiF
Calculated (C)/Estimated (E)		E	E	C	—	C	E	C
Target/kV^{-1}/mA^{-1}		Mo/50/200	Au/?/?	W/?/?		Au/24/200	Mo/23/30	?/?/?
B. XANES								
Photons s^{-1}/energy (eV)		—	—	—	—	5×10^4/ 8980	3.7×10^5, 8980	?
Crystal		—	—	—	—	Si(333)/JS	Ge(333)/JS	Si(440)/JS
Scantime (h)		—	—	—	—	2–3 h	1 h	5 h
Detectors								
Gas proportional counter	(G)	G	G	—	G	—	—	—
Scintillation	(S)	—	—	—	—	S (NaI)	S (NaI)	S
Ionization chamber	(I)	—	—	I	I	I	I	—

Values for the resolution at a certain energy are classified into three categories: (a) determined via measurements of a particular excitation line, (b) calculated via different theoretical approaches, and (c) estimated values. Some authors calculated the photon flux at a certain energy from the measurement of the current produced by the ionization chambers. Others estimated the photon flux probably from the statistics of the experimental data. Sometimes authors indicated that components of their EXAFS apparatus were commercially obtained. This is also mentioned in Table 5.3. In some papers laboratory EXAFS data have been compared with synchrotron EXAFS data. These results will be discussed in Section 5.6.1.

Table 5.3 makes clear that a standard x-ray tube can be used as a source for an EXAFS spectrometer with curved crystals. Stern (34) showed that a photon flux of about 5×10^5 s^{-1} can be obtained at the copper-edge with a resolution of 5 eV using a Si(400) crystal. Measurements were carried out with ionization chambers as detectors. Williams (7) claimed fluxes of 6×10^6 s^{-1} with a resolution of 10 eV at the copper-edge by utilizing a Ge(111) Johansson monochromator (127 mm horizontal spotwidth) and a NaI scintillation detector. His x-ray source is a standard molybdenum-tube (2 kW).

Most spectrometers utilize a rotating anode as an x-ray source. Good resolutions with relatively high intensities were obtained by Thulke et al. (8). With a Rigaku RU 200 x-ray source and a Ge(311) Johansson monochromator crystal (40-mm horizontal spot width) they measured 5×10^6 photons s^{-1} within a bandpass of 4.5 eV at an energy of 8.2 keV. Very high intensities with a moderate resolution were reported by Brinkgreve et al. (30). Using the linear spectrometer especially designed for the Elliot type GX 21 rotating anode (see also Section 5.5.1) and a Si(111) Johansson monochromator crystal (70-mm horizontal spot width) a resolution of 11 eV was measured with an intensity of 3×10^7 photons s^{-1} at the copper *K*-edge.

5.5.3. Optimization

Table 5.3 makes clear that a large range of intensities (10^4–10^6 photons s^{-1}) and energy resolutions (2–15 eV) have been accomplished by the laboratory EXAFS spectrometers described in recent literature. Some spectrometers are able to produce photon fluxes in the order of 5×10^6 photons s^{-1} with resolutions of about 5 eV. It was demonstrated in Section 5.2.1 that a large class of experiments ($\mu_s/\alpha\ \Delta\mu_s \approx 500$, $S/N \approx 100/1$) can be carried out with a minimum useful photon flux of about 3×10^6 photons s^{-1} accepting a total scan time of 20 h (counting time per data point 100 s). Williams (7) has shown that acceptable results can be obtained with a Ge(111) Johansson crystal that could be fabricated with a horizontal size of 127 mm. Therefore, the spectrom-

eter described by Thulke et al. (8) could be further optimized by using a Ge(311) Johansson crystal with a larger horizontal spot width (40 → 120 mm) resulting in a flux of 1.5×10^7 photons s^{-1} at 8.2 keV (resolution 4.5 eV). The spectrometer of Brinkgreve et al. (30) might produce at 9 keV an intensity of about 2×10^8 photons s^{-1} (resolution 11 eV) by using a gold anode (Mo → Au, increase ~1.6×) and a Ge(111) monochromator crystal (rocking curve, increase ~2.5×) with a horizontal spot width of 120 mm (70 → 120 mm, increase ~ 1.7×). By changing the type of germanium crystal [Ge(311) → Ge(111)] the optimized spectrometer of Thulke et al. (8) can give a higher number of photons (~5.3×10^7 s^{-1}) with a lower resolution. Conversely the optimized spectrometer of Brinkgreve et al. (30) will produce a lower intensity (~5.7×10^7 s^{-1}) with a higher resolution when using a Ge (311) crystal. The calculations are based upon data, which are derived from real experiments and show that optimized laboratory EXAFS facilities can give photon fluxes that are 10–15 times larger than the fluxes mentioned in the literature until now. Resolutions will then be in the order of 10 eV, which are acceptable for deriving reliable structural information (see also Sections 5.2.1 and 5.6.1).

Not only the photon flux, but also the reliability and the feasibility of laboratory EXAFS spectrometer have to be improved further. Such improvements, together with an optimization of the actual photon flux may lead to a situation where the laboratory EXAFS facility is competitive for a large class of experiments with an EXAFS station at a synchrotron beamline. In the following, attention will be paid to the different components of the laboratory spectrometer, which have to be improved further.

A high quality Johansson-type curved monochromator crystal of large (horizontal) dimension (100–150 mm) forms the key of such an improvement. As already mentioned, normally cylindrical-type Johansson crystals with horizontal dimension of 127 mm have been fabricated (7). Very promising results have been obtained with double curved crystals (31), which can focus more photons in the vertical plane leading to higher x-ray intensities of the sample. The best material for EXAFS monochromator crystals is germanium due to its larger rocking curves. However, germanium is only useful for energies lower than 11 keV, due to the position of its *K*-edge at 11.103 keV.

A point of further concern is the rotating anode, which should be used as an x-ray source in an optimized laboratory instrument. At low excitation voltages high currents have to be realized with a current regulation circuit of high quality to allow optimum short term stability. The high voltage circuit must be protected against an electronic discharge in the vacuum chamber of the anode. The high voltage has to be switched on again automatically after such an event, allowing long scan times also during nighttime. The housing of the rotating anode must be constructed in such a way that long lifetimes of the bearings are normal.

Magnetic fluid vacuum seals are recommended at present, because they guarantee good vacuum conditions. Since the anode focal spot has to be aligned together with the Rowland circle mechanism, the repositioning of a new filament and its focal cup and also the exchange of different types of anodes must be possible without new alignment procedures.

5.6. LABORATORY VERSUS SYNCHROTRON EXAFS FACILITIES

5.6.1. Comparison of Results on Both Types of Facilities

Information, which might be of great help to get an objective opinion about the actual capabilities of laboratory EXAFS spectrometers consists of a comparison of data obtained on the same sample with a laboratory as well as a synchrotron EXAFS facility. Khalid et al. (16) compared the Fourier transforms of EXAFS data obtained for nickel foil measured on their laboratory spectrometer and on EXAFS station I-5 at SSRL (ring conditions: 2.66 GeV, 60 mA). The Fourier transforms measured on both facilities have the coordination peaks at the same distances (Fig. 5.21). However, the magnitude of the peaks of the Fourier transform of the data collected on the laboratory spectrometer are lower than for the synchrotron EXAFS data. The peak corresponding to the first coordination distance is about 20% lower, whereas the peak of the third shell decreased by about 27%. The SSRL data were taken with a resolution of about 1–2 eV. The authors measured the resolution of their laboratory EXAFS spectrometer to be 6.2 eV at the tungsten $L_{\alpha 1}$ line (8397.6 eV). The convolution calculations of Section 5.2.2.2 show that resolutions of about 20 eV will degrade the first-shell peak by about 20%. Peaks for higher coordination distances decrease much more than 27%, as found for the third shell of the nickel foil data measured on the Delaware spectrometer. This problem has been mentioned already by Stern (4) in his comments on these results. He alluded thickness effects (34) as possible origins for these amplitude differences.

A more detailed comparison of EXAFS data measured on laboratory and synchrotron facilities has been made by van Zon (11). Figure 5.22(*a*) and 5.22(*b*) show the x-ray absorption spectrum and the EXAFS of platinum metal foil, measured on beamline *I*-5 (SSRL), [Si(220) channel cut, resolution 2–3 eV, dedicated operation 3 GeV and 40 mA]. The absorption spectrum was recorded in one scan of 35 min. The actual photon flux at the sample is unknown. In Fig. 5.22*c* and *d* the measurements, performed with the Eindhoven EXAFS spectrometer (30), are presented. The measurements were carried out using a Si(400) monochromator with the x-ray generator operating at 240 mA and 21 kV, thus avoiding higher harmonics. The measured resolution was 11.2 eV,

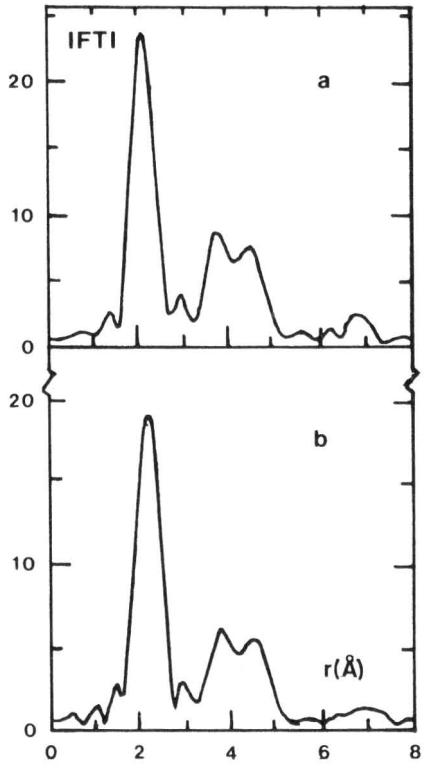

Figure 5.21. Fourier transforms (magnitude |FT|) of Ni foil (E = 8.3 keV) measured both at SSRL (*a*) and on the laboratory spectrometer of the University of Delaware (*b*).

while the intensity was estimated to be 3.10^5 photons s^{-1} (2-mm spot width). To get a good signal-to-noise ratio a scan of 15 h was made. There exists a difference between the two absorption spectra in intensity of the white line and in amplitude of the EXAFS signal at low-k-values. To compare the quality of the EXAFS data, a k^2-weighted Fourier transform was performed on both EXAFS functions. By using a high weight factor the difference at low k values are suppressed and thus the influence of the resolution if minimized.

In Figure 5.22(*e*) the k^2-weighted Fourier transforms on both data sets are displayed. The transforms look very similar and the amplitude of the peaks, for the higher coordination shell as well, hardly differ in amplitude. A more quantitative comparison was obtained by convolution of the SSRL data with a Gaussian energy distribution function. A full width at half-maximum (FWHM) value of 7 eV of the Gaussian resolution function applied to the SSRL data resulted in a good agreement with the laboratory EXAFS data (see Fig. 5.22*f*). This is a strong indication that no artifacts caused by the laboratory spectrometer are

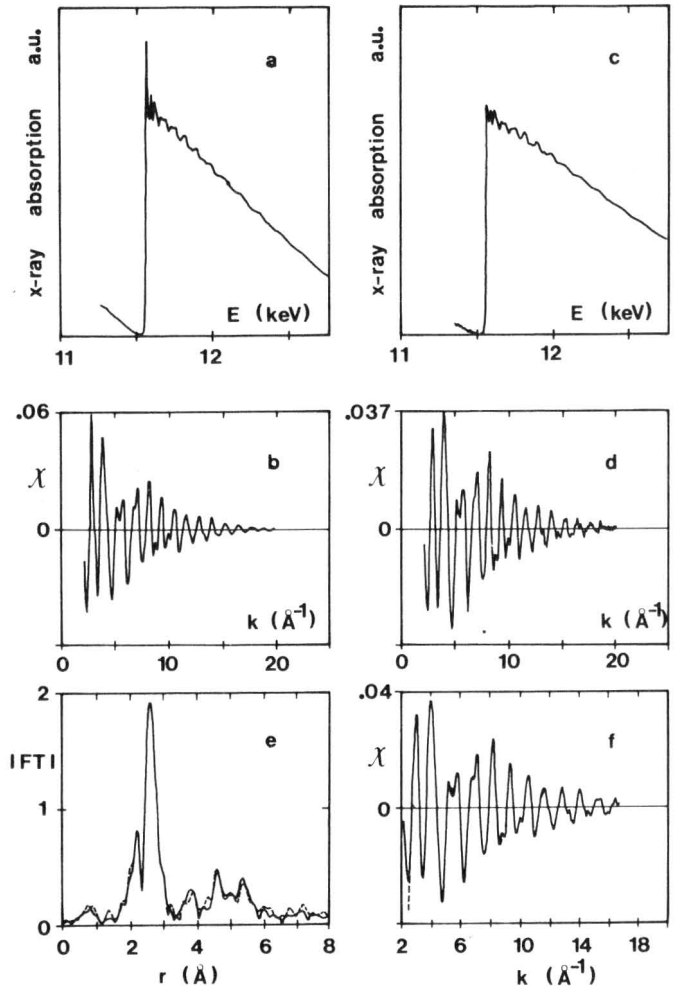

Figure 5.22. Data of Pt-foil collected at the L_{III}-edge (E = 11.564 keV): (*a*) X-ray absorption spectrum, measured at SSRL; (*b*) EXAFS spectrum (SSRL); (*c*) X-ray absorption spectrum, measured on the Eindhoven EXAFS facility; (*d*) EXAFS spectrum (lab. EXAFS); (*e*) Fourier transforms (k^2, Δk = 2.6–19 Å^{-1}) of the EXAFS spectra shown in (*b*) (solid line) and d (dashed line); and (*f*) EXAFS data (laboratory EXAFS solid line, convoluted SSRL data dotted line).

present in the EXAFS data. According to the convolution procedure, the SSRL data should have been measured with a resolution of 8.7 eV. This value is quite large for the channel-cut Si(220) monochromator (vertical divergence is 5×10^{-5} rad). However, the SSRL spectrum was measured with a ring energy of 3 GeV and at this energy there is a significant contribution of higher harmonics radiation that is not rejected by the channel-cut Si(220) monochromator. This could explain the differences between the SSRL calculated apparent and the real energy resolution. The results presented in this paragraph make clear that high quality EXAFS data can be obtained on laboratory EXAFS spectrometers. As already discussed in Section 5.2.2.2 a resolution of about 10 eV can be taken as a maximum value to derive reliable information about higher coordination shells.

5.6.2. Analysis of Laboratory EXAFS Data

A full analysis of high quality EXAFS data collected with laboratory EXAFS spectrometers has been presented in the recent literature by Thulke et al. (35, 36), Tohji et al. (37), and Kampers et al. (38). As an example, the EXAFS study of Kampers et al. will be discussed in more detail. They studied with the EXAFS spectrometer described in (30) the influence of the method of preparation on the size of platinum metal crystallites supported on ZSM-5 zeolite. Details of the preparation are given in ref. (38). EXAFS measurements were carried out at room temperature on the platinum L_{III}-edge after passivation (cooling down in flowing H_2 to room temperature and subsequently slowly introducing a mixture of dioxygen and helium). The resolution of the Si(400) monochromator at the platinum-edge was 14 eV with an x-ray spot size on the crystal of 10 (vertical) $\times$ 20 mm (horizontal). The x-ray generator operated at 21 kV and 240 mA producing a photon flux of about 3×10^6 photon s^{-1} at the sample. Collection times were in the order of 22 h. The EXAFS spectra of a 4.7 wt.% (preparation via impregnation) and a 9.4 wt.% (preparation via ion exchange) Pt/ZSM-5 catalyst are presented in Fig. 5.23*a* and *b*, respectively. Due to the passivation procedure it is likely that Pt–Pt and Pt–O bonds are present in the EXAFS spectra. A k^3-weighted Fourier transform (corrected for the Pt–Pt phase shift and backscattering amplitude [see also ref. (10)] gives the best separation between the Pt–Pt and the Pt–O bonds. In a Pt–Pt phase corrected Fourier transform the Pt–Pt contribution peaks at the actual coordination distance (in the transforms of both catalysts at 2.77 Å) (see Fig. 5.22*c*, *d*, *e*, and *f*). Pt foil and $Na_2Pt(OH)_6$ were measured under the same experimental conditions in order to obtain phase shift and backscattering amplitude functions for the analysis of the Pt–Pt and Pt–O absorber–scatterer pairs. By applying the "difference

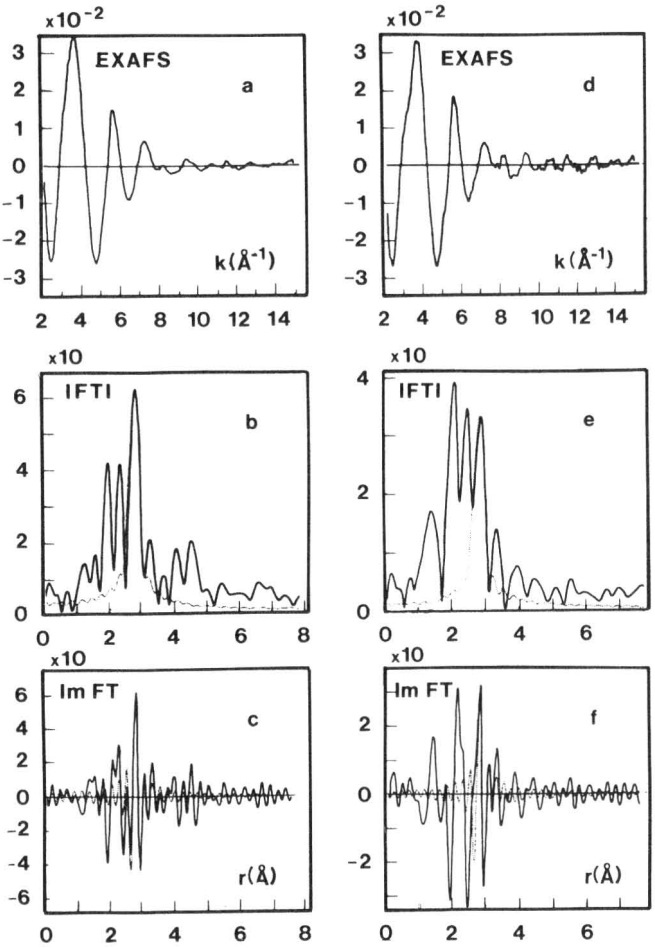

Figure 5.23. EXAFS data measured at the L_{III}-edge of Pt/ZSM-5 catalysts on the Eindhoven EXAFS facility. EXAFS spectrum of (*a*) 4.7 wt.% Pt/ZSM-5 (impregnation) and (*d*) 9.4 wt.% Pt/ZSM-5 (ion exchange). Magnitudes (|FT|) (*b* and *e*) and Imaginary parts (Im FT) (*c* and *f*) of Fourier transforms (k^3, Δk = 2.9–14 Å^{-1}, Pt—Pt phase and amplitude corrected) of EXAFS spectra (*a*) and (*b*), respectively.

file'' technique (11) the following Pt–Pt coordination parameters were obtained: $N = 5.5$, $R = 2.7$ Å, $\Delta 6^2 = 0.003$ Å^2 (sample prepared via impregnation); $N = 2.9$, $R = 2.77$ Å, $\Delta 6^2 = 0.003$ Å^2 (sample prepared via ion exchange). The Fourier transform (Pt–Pt phase and amplitude corrected) of an EXAFS function calculated with these parameters (dotted lines in Fig. 5.23*c*, *d*, *e*, and

f) gives for both catalysts a Pt–Pt peak that superimposes the Pt–Pt peak in the Fourier transform of the experimental data. From this EXAFS study the authors were able to conclude that the impregnation method leads to much larger platinum crystallites on the *ZSM*-5 support than the ion exchange method. These results and the results of the analysis of the other laboratory EXAFS data published in the literature (35–37) clearly show that reliable structural information can be obtained from laboratory EXAFS data if the quality of the EXAFS data is comparable with good quality EXAFS data obtained with a synchroton EXAFS facility.

5.6.3. Optimal Use and Advantages of Laboratory and Synchrotron EXAFS Facilities

The useful energy range of in-house EXAFS spectrometers is limited to $4 \leq E \leq 20$ keV, while the lowest concentration that can be measured is in the order of 25–50 m*M*. There are also limitations on the type of experiments, which can be performed on laboratory EXAFS systems. EXAFS fluorescence experiments on very dilute samples (1–10 m*M*), polarization studies, time-dependent measurements (using dispersive EXAFS), and experiments, which need highly intense collimated x-ray beams (surface studies) can only reliably be carried out on dedicated synchrotron EXAFS stations. However, for all other type of experiments that are not limited by the energy and concentration ranges mentioned previously, the laboratory EXAFS facility might be fully competitive with a synchrotron EXAFS station. This is only the case if the laboratory facility is optimized according to the points discussed in Section 5.5.3.

A lot of EXAFS data that nowadays are collected on EXAFS stations of synchrotron beamlines could be measured by experimentalists with their own EXAFS facility. Most users of synchrotron facilities will have the experience that 20–40% of the allocated beamtime is lost by injection procedures, machine failures, and ring instabilities. Already today the demand for EXAFS beamtime on synchrotron facilities can hardly be satisfied and there is still a growing interest in doing EXAFS experiments. It should therefore be advantageous for the whole EXAFS community if only those EXAFS experiments that really need the broad energy range, the polarization, and the high intensity or synchrotron radiation, are carried out at synchrotron EXAFS stations, thus relieving this type of EXAFS facility.

The roles of in-house and synchrotron EXAFS facilities have been extensively discussed during the workshop organized by Professor Stern (4). Since 1980 new technologies diminished the limitations of laboratory EXAFS facilities and new prospectives for these facilities have become clear. Most of these prospectives have been discussed in the previous sections. It seems worthwhile

to mention here for both types of facilities those advantages, which are timeless: Synchrotron EXAFS facility:

- Broad photon energy range.
- High intensities together with high resolutions.
- Education of students by interactions with outstanding scientists, who are doing sophisticated experiments also on other types of synchrotron stations.

Laboratory EXAFS facilities:

- Setting of priority by experimenters.
- Much faster and better interaction between experiment and follow-up leading to new ideas and new experiments.
- Much easier to carry out experiments that need complicated facilities for sample preparation and *in situ* experiments.
- Rapid implementation of ideas.
- Excellent teaching and training possibilities for students.
- Avoidance of travel expenses.

For industries the possibilities for proprietary research are unlimited and no problems will arise in obtaining high ratings for beamtime from the proposal panel review for more routinelike research.

5.7. SUMMARY AND CONCLUSIONS

This chapter has demonstrated that high quality XANES and EXAFS spectra can be collected with laboratory EXAFS facilities. The limitations of these facilities have been discussed and it has been shown that synchrotronlike resolutions, which are sometimes claimed by enthusiastic supporters of synchrotron facilities to be essential for deriving reliable structural EXAFS information, are not necessary. Resolutions of 10–15 eV can still be expected. XANES spectra can be measured with synchrotronlike resolutions within an acceptable time of 1–2 h.

At this moment only a few papers dealing with the analysis of high quality laboratory EXAFS data have been published. Laboratory EXAFS spectrometers, fully optimized according to the points discussed in Section 5.5.3, have not yet been reported in the literature. A key point in this optimization process is the production of high quality monochromator crystals of large (horizontal) dimen-

sions. No large scale applications for laboratory EXAFS facilities are foreseen, if this optimization does not take place and if intensities impinging on the sample remain lower than 10^7 photons s^{-1} (bandpass 5–15 eV). However, the technologies available nowadays can bring such an optimization to reality and many experimentalists may then make fruitful use of their laboratory EXAFS facility.

ACKNOWLEDGMENTS

The author gratefully acknowledges the many fruitful discussions with Dr. J. B. A. D. van Zon, Ir. P. Brinkgreve, T. J. M. Maas, and Dr. M. P. A. Viegers. The author is also thankful for the encouragement and stimulating discussions with Professor E. A. Stern and Professor D. E. Sayers.

REFERENCES

1. P. A. Lee, P. H. Citrin, P. Eisenberger, and B. M. Kincaid, *Rev. Mod. Phys.*, **53,** 805 (1981).
2. R. Cortes, private communication.
3. J. A. Del Cueto and N. J. Shevchik, *J. Phys. E*, **11,** 1 (1978).
4. Laboratory EXAFS Facilities, *AIP Conference Proceedings No. 64*, E. A. Stern (Ed.), American Institute of Physics, New York, 1980.
5. L. Incoccia and S. Mobilio, in *EXAFS and Near Edge Structure*, A. Bianconi, L. Incoccia, and S. Stipcich (Eds.), Springer-Verlag, Berlin, 1983, p. 87.
6. W. H. Zachariasen, *Theory of X-Ray Diffraction in Crystals*, 2nd ed., Wiley, New York, 1967.
7. A. Williams, *Rev. Sci. Instrum.*, **54,** 193 (1983).
8. W. Thulke, R. Haensel, and P. Rabe, *Rev. Sci. Instrum.*, **54,** 277 (1983).
9. K. Tohji, Y. Udagawa, T. Kawasaki, and K. Masuda, *Rev. Sci. Instrum.*, **54,** 1482 (1983).
10. D. C. Koningsberger and D. E. Sayers, *Solid State Ionics*, **16,** 23 (1985).
11. J. B. A. D. van Zon, thesis, Eindhoven University of Technology, Eindhoven, The Netherlands, 1984.
12. T. M. J. Maas and P. Brinkgreve, Internal Report, Eindhoven University of Technology, Eindhoven, The Netherlands, 1984.
13. G. R. Fischer, in Laboratory EXAFS Facilities, *AIP Conference Proceedings No. 64*, E. A. Stern (Ed.), American Institute of Physics, New York, 1980, p. 21.
14. M. Prins, Internal Report, Eindhoven University of Technology, The Netherlands, 1984.
15. G. S. Knapp and P. Georgopoulos, in Laboratory EXAFS Facilities, *AIP Confer-*

ence Proceedings No. 64, E. A. Stern (Ed.), American Institute of Physics, New York, 1980, p. 2.

16. S. Khalid, R. Emrich, R. Dujari, J. Schultz, and J. R. Katzer, *Rev. Sci. Instrum.*, **53,** 22 (1983).
17. D. W. Berreman, *Rev. Sci. Instrum.*, **26,** 1048 (1955).
18. J. W. M. Dumond, *Rev. Sci. Instrum.*, **18,** 626 (1947).
19. J. W. M. Dumond, D. A. Lind, and R. E. R. Cohen, *Rev. Sci. Instrum.*, **18,** 617 (1947).
20. N. G. Webb, *Rev. Sci. Instrum.*, **47,** 545 (1976).
21. A. Franks, *J. Appl. Phys.*, **9,** 349 (1958).
22. P. Georgopoulos and C. H. Tang, in *Advances in X-Ray Analysis*, Vol. 27, J. B. Cohen, J. C. Russ, D. E. Leyden, C. S. Barrett, and P. K. Predecki, (Eds.), Plenum, New York, 1984, p. 299.
23. E. A. Stern, in Laboratory EXAFS Facilities, *AIP Conference Proceedings No. 64*, E. A. Stern (Ed.), American Institute of Physics, New York, 1980, p. 39.
24. J. B. A. D. van Zon, Internal Report, Eindhoven University of Technology, The Netherlands, 1984.
25. D. W. Berreman, *Phys. Rev. B*, **19,** 560 (1979).
26. G. S. Knapp, H. Chen, and T. E. Klippert, *Rev. Sci. Instrum.*, **49,** 1658 (1978).
27. B. E. Warren, in *X-Ray Diffraction*, Addison-Wesley, Reading, MA, 1969, p. 46.
28. Kun-quan Lu and E. A. Stern, in Laboratory EXAFS Facilities, *AIP Conference Proceedings No. 64*, E. A. Stern (Ed.), American Institute of Physics, New York, 1980, p. 104.
29. J. E. White, *J. Appl. Phys.*, **21,** 855 (1950).
30. P. Brinkgreve, T. M. J. Maas, D. C. Koningsberger, J. B. A. D. van Zon, M. H. C. Janssen, A. C. M. E. van Kalmthout, and M. P. A. Viegers, in *EXAFS and Near Edge Structures III*, K. O. Hodgson, B. Hedman, and J. E. Penner-Hahn (Eds.), Springer-Verlag, Berlin, 1984, p. 517.
31. M. P. A. Viegers, Internal Report, Philips Research Laboratories, Eindhoven, The Netherlands, 1984.
32. P. Georgopoulos and G. S. Knapp, *J. Appl. Cryst.*, **14,** 9 (1981).
33. G. G. Cohen, D. A. Fisher, J. Colbert, and N. J. Shevchik, *Rev. Sci. Instrum.*, **51,** 273 (1980).
34. E. A. Stern and K. Kim, *Phys. Rev. B*, **23,** 3781, (1981).
35. W. Thulke, R. Frahm, R. Haensel, and P. Rabe, *Phys. Status Solidi*, **75,** 501 (1983).
36. W. Thulke, R. Haensel, and P. Rabe, *Phys. Status Solidi*, **78,** 539 (1983).
37. K. Tohji, Y. Udagawa, S. Tanabe, and A. Ueno, *J. Am. Chem. Soc.*, **106,** 612 (1984).
38. F. W. H. Kampers, F. B. M. Duivenvoorden, J. B. A. D. van Zon, P. Brinkgreve, M. P. A. Viegers, and D. C. Koningsberger, *Solid State Ionics*, **16,** 55 (1985).